

DOT/FAA/AR-04/34

Office of Aviation Research
Washington, D.C. 20591

Modeling of a Commuter Category Aircraft Seat

September 2004

Final Report

This document is available to the U.S. public
through the National Technical Information
Service (NTIS), Springfield, Virginia 22161.



U.S. Department of Transportation
Federal Aviation Administration

NOTICE

This document is disseminated under the sponsorship of the U.S. Department of Transportation in the interest of information exchange. The United States Government assumes no liability for the contents or use thereof. The United States Government does not endorse products or manufacturers. Trade or manufacturer's names appear herein solely because they are considered essential to the objective of this report. This document does not constitute FAA certification policy. Consult your local FAA aircraft certification office as to its use.

This report is available at the Federal Aviation Administration William J. Hughes Technical Center's Full-Text Technical Reports page: actlibrary.tc.faa.gov in Adobe Acrobat portable document format (PDF).

1. Report No. DOT/FAA/AR-04/34		2. Government Accession No.		3. Recipient's Catalog No.	
4. Title and Subtitle MODELING OF A COMMUTER CATEGORY AIRCRAFT SEAT				5. Report Date September 2004	
				6. Performing Organization Code	
7. Author(s) Hampton C. Gabler, David Bowen, and Christopher Molnar				8. Performing Organization Report No.	
9. Performing Organization Name and Address Rowan University Department of Mechanical Engineering Glassboro, NJ 08028				10. Work Unit No. (TRAIS)	
				11. Contract or Grant No. 00-G-022	
12. Sponsoring Agency Name and Address U.S. Department of Transportation Federal Aviation Administration Office of Aviation Research Washington, DC 20591				13. Type of Report and Period Covered Final Report	
				14. Sponsoring Agency Code	
15. Supplementary Notes The FAA William J. Hughes Technical Center Project Manager was John Zvanya.					
16. Abstract <p>This report describes the development of a nonlinear finite element model of a commuter category aircraft seat designed to explore the issue of energy absorption in severe, but survivable, crashes. The research program used a Beechcraft 1900C passenger seat as a reference commuter category aircraft seat. The report presents a description of the model and the results of finite element modeling of the reference seat at increasingly severe impact velocities. The report also presents the results of a parallel experimental program, conducted to validate the model, in which an instrumented crash dummy was drop tested in the reference seat at the same impact velocities as the simulation. Experimental results are reported for passenger lower lumbar loading, peak pelvic acceleration, and seat structural loading.</p>					
17. Key Words Aircraft crash, Finite element model, Commuter category aircraft, Drop test				18. Distribution Statement This document is available to the public through the National Technical Information Service (NTIS) Springfield, Virginia 22161.	
19. Security Classif. (of this report) Unclassified		20. Security Classif. (of this page) Unclassified		21. No. of Pages 89	22. Price

ACKNOWLEDGEMENTS

The authors wish to acknowledge Gary Frings, John Zvanya, Dr. Tong Vu, and Allan Abramowitz of the Federal Aviation Administration William J. Hughes Technical Center for their support of this research effort. Our thanks as well to the following undergraduate engineering research assistants for their contributions to the project: Alan Courtright, Matthew Hammill, Jeremy Lamb, Vern Schwanger, and Mark Seidman.

TABLE OF CONTENTS

	Page
EXECUTIVE SUMMARY	xi
1. INTRODUCTION	1-1
2. OBJECTIVE	2-1
3. RESEARCH APPROACH	3-1
4. GEOMETRIC MODELING OF THE AIRCRAFT SEAT	4-1
4.1 Seat Selection	4-1
4.1.1 Seat Performance in Previous Tests	4-1
4.1.2 Seat Availability	4-1
4.1.3 Modeling Considerations	4-1
4.1.4 Selection	4-2
4.2 Seat Teardown	4-3
4.2.1 Canvas and Padding	4-3
4.2.2 Frame	4-4
4.2.3 Pegs	4-7
4.2.4 Measurement of the Frame Internal Geometry	4-7
4.2.5 Material Properties	4-7
4.3 Solid Model	4-7
4.3.1 Three-Dimensional Model	4-8
4.3.2 Seat Base	4-8
4.3.3 Seat Back	4-9
4.3.4 Leg Bar	4-9
4.3.5 Stabilizer Bar	4-9
4.3.6 Bolts	4-10
4.3.7 Pegs	4-10
4.3.8 Three-Dimensional Assembly	4-10
4.4 Conversion to Shell Model	4-11
5. DEVELOPMENT OF THE FINITE ELEMENT MODEL	5-1
5.1 Mesh Generation	5-1
5.1.1 Importing Geometric Model From SolidWorks	5-1

5.1.2	Positioning Parts	5-1
5.1.3	Collectors	5-2
5.1.4	Meshing	5-2
5.1.5	Solid Elements	5-3
5.1.6	Shell Elements	5-3
5.2	Development of the LS-DYNA Model	5-4
5.2.1	Keywords and Cards	5-4
5.2.2	Setup With HyperMesh	5-4
5.2.3	Simulation	5-5
5.2.4	Postprocessing	5-5
5.2.5	Loading Conditions	5-6
5.2.6	Boundary Conditions	5-7
5.2.7	Initial Conditions	5-7
5.2.8	Contacts	5-7
5.2.9	Element Formulation	5-8
5.2.10	Material Types	5-8
5.2.11	Control Cards	5-8
5.2.12	Modeling the Dummy	5-8
5.2.13	Constitutive Properties for Seat Model	5-9
5.2.14	Minimizing Simulation Run Times	5-10
6.	DROP TOWER TESTING	6-1
6.1	Overview of the Rowan University Drop Test Facility	6-1
6.2	Description of the Drop Tower	6-2
6.2.1	Drop Tower	6-2
6.2.2	Seat Platform	6-2
6.2.3	Hoist and Quick Release Mechanism	6-3
6.2.4	Impact Block	6-4
6.3	Test Items	6-5
6.3.1	Anthropomorphic Test Device	6-5
6.3.2	Surrogate Test Seat	6-6
6.3.3	Instrumentation	6-6
6.3.4	Data Acquisition Systems	6-8
6.3.5	Kodak MotionCorder	6-8
6.4	Results	6-9
7.	IMPACT SIMULATIONS	7-1
7.1	Approach	7-1
7.2	Comparison of Simulated Drop Tests With Experimental Results	7-1

8.	SUMMARY	8-1
9.	REFERENCES	9-1

APPENDICES

- A—Test Report for 1-Meter Drop Tower Test of a Beechcraft 1900C Passenger Seat
- B—Test Report for 1.5-Meter Drop Tower Test of a Beechcraft 1900C Passenger Seat
- C—Test Report for 2-Meter Drop Tower Test of a Beechcraft 1900C Passenger Seat

LIST OF FIGURES

Figure		Page
1-1	Federal Aviation Administration Drop Test of a Boeing 737 Test Section	1-1
4-1	Beechcraft 1900C Passenger Seat	4-2
4-2	Seat Bottom Cushion With Covering Removed	4-3
4-3	Cutaway of Seat Bottom Cushion Showing Seat Pan	4-4
4-4	Seat Frame With One Segment of the Seat Base Removed for Material Testing	4-4
4-5	Seat Base Frame	4-5
4-6	Seat Back Frame	4-5
4-7	Leg Bar Frame	4-6
4-8	Stabilizer Bar Frame	4-6
4-9	Peg Connection Between Seat Base and Leg Bar	4-7
4-10	Geometric Model of the Reference Seat	4-10
5-1	HyperMesh Model of the Reference Seat	5-2
5-2	LS-DYNA Model of Reference Seat Showing Stresses in a Trial Run	5-6
5-3	Beechcraft Seat Model With the Dummy FE Model	5-9
6-1	The Rowan University Drop Tower	6-1
6-2	Instrumented Crash Test Dummy Seated in the Rowan University Drop Tower	6-2
6-3	Seat Platform Fixture	6-3
6-4	Hoist and Quick Release Mechanism	6-4
6-5	Impact Block for Rowan University Drop Tower	6-4
6-6	Hybrid II Crash Test Dummy	6-5
6-7	Surrogate Seat for Drop Tower Checkout Tests	6-6
6-8	Kodak MotionCorder High-Speed Digital Video Recorder	6-9
6-9	Seat and Dummy Assembly at Drop Heights Just Prior to Drop Testing	6-11
7-1	Pelvis Acceleration, 1-Meter Drop, Filtered Using a Class 60 Filter	7-2
7-2	Lumbar Load, 1-Meter Drop, Filtered Using a Class 60 Filter	7-3
7-3	Pelvis Acceleration, 1.5-Meter Drop, Filtered Using a Class 60 Filter	7-3
7-4	Lumbar Load, 1.5-Meter Drop, Filtered Using a Class 60 Filter	7-4
7-5	Pelvis Acceleration, 2-Meter Drop, Filtered Using a Class 60 Filter	7-4
7-6	Lumbar Load, 2-Meter Drop, Filtered Using a Class 60 Filter	7-5

LIST OF TABLES

Table		Page
5-1	Constitutive Properties	5-9
6-1	Drop Test Instrumentation (Sensors)	6-7
6-2	Drop Test Matrix	6-9
6-3	Drop Test Peak Measurements—Absolute Value	6-10

LIST OF ACRONYMS

3D	Three-dimensional
A/D	Analog-to-digital
ALE	Arbitrary Lagrangian-Eulerian
DAQ	Data acquisition system
FAA	Federal Aviation Administration
FE	Finite element
fps	Frames per second
PC	Personal computer
psi	Pounds per square inch

EXECUTIVE SUMMARY

This report describes the development of a nonlinear finite element model of a commuter category aircraft seat designed to explore the issue of energy absorption in severe, but survivable, crashes. The research program used a Beechcraft 1900C passenger seat as a reference commuter category aircraft seat. The report presents a description of the model and the results of finite element modeling of the reference seat at increasingly severe impact velocities. The report also presents the results of a parallel experimental program, conducted to validate the model, in which an instrumented crash dummy was drop tested in the reference seat at the same impact velocities as the simulation. Experimental results are reported for passenger lower lumbar loading, peak pelvic acceleration, and seat structural loading.

1. INTRODUCTION.

The Federal Aviation Administration (FAA) William J. Hughes Technical Center has undertaken an extensive research program to explore and maximize the crash survivability of aircraft in severe, but survivable, crashes. Using the FAA Dynamic Vertical Drop Test Facility, the FAA researchers have conducted full-scale tests in which an aircraft cabin containing instrumented crash dummies were subjected to vertical impact velocities up to 30 ft/sec (figure 1-1). Previous tests have included a Beechcraft 1900C Airliner [1], a Shorts 330 Airliner [2], a Metro III Aircraft [3], and several Boeing 737 fuselage sections [4]. These tests have demonstrated a significant probability of severe lower lumbar injury at these velocities.

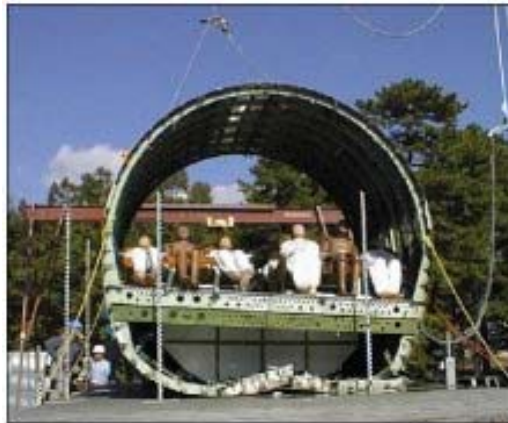


FIGURE 1-1. FEDERAL AVIATION ADMINISTRATION DROP TEST OF A BOEING 737 TEST SECTION

More recently, Rowan University, in collaboration with the FAA, has conducted a series of aircraft seat drop tests to compare and contrast the relative survivability of three different commuter category aircraft seat designs. Using the Rowan University Drop Tower, these component tests have shown significant differences in the ability of individual seat designs to protect their occupants from serious spinal injury.

What is not clearly understood, however, are the nature of the engineering design features that led to seat failure for some designs and crash survivability for other seat designs. Clearly, if these design differences could be more fully understood, the more successful design features could be incorporated into future seat designs as a means of reducing crash related passenger injuries. Although experimental tests are extremely valuable as a means of determining the relative crashworthiness of different aircraft designs, these tests do not, in general, provide the level of engineering insight necessary for seat redesign.

These insights can best be developed only through the development and execution of detailed structural models of the aircraft seat under impact loading. Development of a structural model would allow prediction of structural impact response at impact conditions other than those directly tested, including simulations of crash response from different vertical impact velocities, alternate impact orientations, and multiple passenger sizes. Such a model would also serve as one component of a whole aircraft model for simulation of more complex crash events.

2. OBJECTIVE.

The objectives of the research program were to develop and validate a comprehensive finite element structural model of a production commuter category aircraft seat under impact loading. The resulting model will serve as a computational tool for the future evaluation and development of energy-absorbing seats for commuter category aircraft.

3. RESEARCH APPROACH.

The objective of the research program is to develop a finite element (FE) model of an aircraft seat using the LS-DYNA computer code. LS-DYNA is a general-purpose, explicit finite element program used to analyze the nonlinear dynamic response of three-dimensional (3D) structures. The code is used extensively to model the response of passenger vehicles and occupants to crash loading. LS-DYNA has unique solution procedures that allow the code to simulate the physical behavior of 3D structures: nonlinear dynamics, thermal, failure, crack propagation, contact, quasi-static, Eulerian, arbitrary Lagrangian-Eulerian (ALE), fluid structure interaction, real-time acoustics, and multiphysics coupling.

The research team used the following approach to conduct the research effort:

1. Seat Selection. At the suggestion of the FAA, a Beechcraft 1900C passenger seat was chosen as a reference seat for the modeling and testing effort. An earlier impact test had shown that the Beechcraft 1900C seat was particularly capable of protecting the passenger from excessive lower lumbar loads. The FAA also had sufficient numbers of this seat for drop testing.
2. Seat Teardown and Measurement. The research team dismantled and performed detailed geometric measurements of the reference seat in support of the FE model.
3. Geometric Modeling of the Aircraft Seat. Using the seat geometry developed during the seat teardown, the research team developed a 3D solid model of the reference aircraft seat. The model was developed using the 3D modeler SolidWorks for export into LS-DYNA.
4. Development of a Finite Element Model. Using the SolidWorks representation of the seat, the research team created a finite element mesh of the seat using the HyperMesh code. HyperMesh is an industry-standard finite element pre- and postprocessor that works seamlessly with LS-DYNA and other finite element codes. The HyperMesh FE mesh along with boundary conditions, loads, and constitutive properties was assembled into a finite element model for input to the LS-DYNA code.
5. Drop Tower Tests. The model was validated against impact tests of the reference seat. Drop tests of the reference seat were conducted at heights of 1 meter, 1.5 meters, and 2 meters at the Rowan University Drop Tower. An instrumented crash test dummy was seated in each test to provide occupant injury measurements. Each test required one undamaged reference seat. The seats were provided by the FAA William H. Hughes Technical Center.
6. Impact Simulations. Simulations of the drop tower tests described above were conducted using the FE model. A simulation was also conducted of a fuselage test of a Beechcraft 1900C performed at the FAA William J. Hughes Technical Center.

4. GEOMETRIC MODELING OF THE AIRCRAFT SEAT.

This section describes the development of a 3D geometric model of the reference aircraft seat. The discussion presents the methodology for the selection, teardown, and the 3D geometric modeling of the reference seat.

4.1 SEAT SELECTION.

The first task in the project was to select the aircraft seat for the modeling and testing effort. In consultation with the FAA, the seat was selected according to the following criteria: (1) performance of the seat in previous tests, (2) availability of the seat for additional testing, and (3) modeling considerations.

4.1.1 Seat Performance in Previous Tests.

The FAA and Rowan University considered two different approaches when selecting the reference seat. One approach, the worst-case approach, would select a seat that had been shown to be particularly poor at protecting the passenger from injury in a crash. The alternative, the best-case approach, would select a seat that was already in production and had been shown in FAA tests to be particularly effective in protecting the passenger. As the longer-term goal of this modeling exercise is to study improvements to production seats, the FAA and Rowan University believed that the better approach was to model the better seat. It was believed that a better performing production seat would serve as an excellent starting point for future design improvements.

A previous FAA full-scale fuselage drop test had shown that Beechcraft 1900C commuter aircraft seats were particularly effective at protecting passengers in severe, but survivable crashes. The FAA tested two versions of the Beechcraft 1900C passenger seat: a low seat back version of the seat and a high seat back version. Before this project began, Rowan University performed several trial 0.5-meter drop tests of both seats with an instrumented dummy and found that the low seat back version of the seat resulted in lower lumbar loads. The Beechcraft low seat back version appeared to be a good candidate for the research program.

4.1.2 Seat Availability.

The project was expected to require a total of five seats of any one type. One seat would be reserved for teardown during geometric modeling of the seat and three to four seats would be needed for the drop tests. The plan was to select the seats from the FAA William J. Hughes Technical Center inventory rather than incur the cost of purchasing new seats. The FAA provided all seats to Rowan University. Sufficient seats were available to proceed with the Beechcraft 1900C low seat back.

4.1.3 Modeling Considerations.

The computer model will be validated against the results of a FAA full-scale fuselage drop test and a series of drop tests to be conducted at the Rowan University Drop Tower. It was planned to validate the model against both the test instrumentation measurements and against posttest

physical measurements of seat deformation. Consequently, it was important to select a seat that incurred a measurable deformation in a crash, but did not suffer complete structural collapse.

In a vertical drop test performed by the FAA, standard Beechcraft 1900C seats exhibited these characteristics. The backs of these seats were frequently rotated backward from the impact, and had failed in most cases. Although the seat back failed in the test, the seat pan support structure suffered a modest, but measurable, deformation at the seat connection to the sidewall. Either the high- or low-back Beechcraft 1900C seats would meet this criterion for modeling.

4.1.4 Selection.

At the suggestion of the FAA, a Beechcraft 1900C low-back passenger seat was chosen as the reference seat for the modeling and testing effort. An earlier impact test had shown that this version of the Beechcraft 1900C seat was particularly capable of protecting the passenger from excessive lower lumbar loads. The FAA also had sufficient numbers of this seat for drop testing. Figure 4-1 shows a photograph of the Beechcraft 1900C low-back passenger seat.



FIGURE 4-1. BEECHCRAFT 1900C PASSENGER SEAT

4.2 SEAT TEARDOWN.

Development of the finite element model requires a very detailed geometric description of the seat structure. To obtain this description, a complete teardown, disassembly, and measurement of one of the seats was performed. In addition, coupons were also cut from this seat to determine constitutive properties of the seat structure material. The teardown process is, of course, destructive, and after teardown, this seat was no longer available for testing. However, four additional seats for the actual drop tests were available.

4.2.1 Canvas and Padding.

As shown in figure 4-1, the canvas seat covers on the seat base and the seat back were attached with Velcro strips to their respective frame parts. As illustrated in figure 4-2, the canvas covers and the foam padding underneath the canvas seat covers were removed by hand. The seat contained a fabric-like seat pan in the seat base and another in the seat back. These seat pans were adhesively bonded to their respective frame parts and were removed with a razorblade. In most places, the Velcro strips were attached to the seat pan and back pan, not directly to the seat frame. A cutaway of the seat pan can be seen in figure 4-3.



FIGURE 4-2. SEAT BOTTOM CUSHION WITH COVERING REMOVED



FIGURE 4-3. CUTAWAY OF SEAT BOTTOM CUSHION SHOWING SEAT PAN

4.2.2 Frame.

Figure 4-4 shows the seat frame with all fabric removed. The bare frame of the reference seat consisted of four main components. These parts were seat base, seat back, leg bar, and stabilizer bar. The seat base, shown in figure 4-5, is a square frame that the passenger sits directly on top of and contains two side-mounting pegs. The seat back, shown in figure 4-6, is the frame under the back of the seat and is free to rotate on two bolts. The leg bar, shown in figure 4-7, contains the two floor-mounting pegs and is free to rotate on two bolts. The stabilizer bar, shown in figure 4-8, is free to rotate on two bolts and ends with a notch. The leg bar and the stabilizer bar both fold up under the seat base for storage. A small fin on the leg bar fits into the notch on the stabilizer bar for setup. The entire frame is covered by a thick, gray paint.



FIGURE 4-4. SEAT FRAME WITH ONE SEGMENT OF THE SEAT BASE REMOVED FOR MATERIAL TESTING

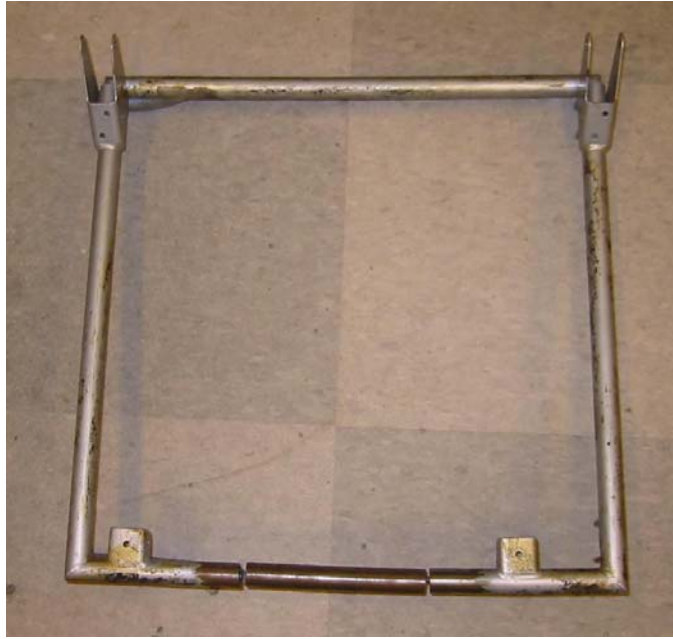


FIGURE 4-5. SEAT BASE FRAME



FIGURE 4-6. SEAT BACK FRAME



FIGURE 4-7. LEG BAR FRAME



FIGURE 4-8. STABILIZER BAR FRAME

These four parts were disassembled by removing the six bolts. The bolts have small, painted nuts on them, possibly making it necessary to use vise grips or pliers for removal. There are also two small washers, one on both ends, on each bolt.

4.2.3 Pegs.

There are four identical pegs in the frame, two connected to the seat base and two connected to the leg bar. Figure 4-9 shows one of the pegs connecting the seat base and the leg bar frame. Each peg consists of a rigid part that is pinned to its respective frame part and attaches to the mounting rail in the airplane. Each peg also has a sliding, spring-loaded cap that aligns the rigid part on the mounting rail. All four of these pegs were removed from the two frame parts to which they were attached. One of these pegs was disassembled further.



FIGURE 4-9. PEG CONNECTION BETWEEN SEAT BASE AND LEG BAR

4.2.4 Measurement of the Frame Internal Geometry.

The frame consists of tubular members with the exceptions of the mounting brackets on the seat base for the three other frame parts and the fin on the leg bar. All subparts are welded together. Inner diameters of these tubes could not be determined from an external inspection. A piece of the seat base frame was removed to allow measurement of the tube wall thickness and inner tube diameter. The frame sample was used later to determine material properties.

4.2.5 Material Properties.

The original belief was that the frame was made of aluminum or an aluminum alloy. The large piece that was removed from the seat base for measurement purposes was used to determine the material of the frame. The paint was removed from this piece, and it was weighed. The volume was calculated from its dimensions. The material's density matched the density of steel almost exactly, therefore, it is assumed that the frame is made of steel. The sample was also found to be attracted to a magnet, which is consistent with a ferromagnetic material such as steel.

4.3 SOLID MODEL.

SolidWorks is a 3D solid geometric modeling program capable of recording and displaying 3D parts in various orientations. All parts were drawn in SolidWorks 2000, including seat base, seat back, leg bar, stabilizer bar, the bolts, and the pegs.

4.3.1 Three-Dimensional Model.

Measurements of the parts were taken as needed and entered into SolidWorks. Geometric modeling of the seat was very detailed to minimize any later simulation errors due to geometric inaccuracies. The detail also increased the visual fidelity of the computer model seat for later comparison with the actual seat.

4.3.2 Seat Base.

The seat base was drawn in four major steps. The four main support members that form the square were drawn using reference geometry and the basic extrusion command. Two reference planes were set up to run parallel with the four intersections between each member. Two more reference planes were set up to run parallel with the cross sections of the members and to intersect each member roughly in the middle of its length. It was necessary to make three extrusions, because SolidWorks 2000 does not allow disjoint components of the same part. After the cross-section of each member was sketched, it was extruded “up to surface” to the respective reference plane.

The next step was to draw the mounting arms and the reinforcement plate attached to the larger mounting arm. Both mounting arms were curved, so spline extrusions were necessary. A reference plane was set up to run parallel with the would-be side-mounting rail, at the correct distance from the edge of the part. Two separate 3D curves were run from the reference plane to the respective location of the part. Two separate spline extrusions were extruded along the 3D curves to form the mounting arms of the seat base. Since the spline extrusion option cannot be complete up to surface, it was necessary to trim the excess by making a cut inside the two main support members to which the mounting arms attached. The reinforcement plate was drawn by sketching the small, exposed, outer surface of the plate (of the three exposed surfaces, two are large, one is small) and then extruding it up to surface to the larger mounting arm.

There are four identical mounting brackets. Both pairs were drawn the same way. A reference plane was set up to run parallel with the outer U-shaped (or C-shaped) surface. The sketch was done on the reference plane and extruded up to surface to the seat base. Each mounting bracket has two holes; each pair of brackets has four holes, which were cut at the same time. The other pair was created the same way.

There are two mounting brackets for the seat back, which are called fins. The welds that connect the fins to the seat base frame were not as straightforward to draw as the rest of the welds. The fins were first drawn using reference geometry and extrusions, much like the rest of the model. The fins were drawn disconnected from the seat base frame by attaching them to the frame temporarily with an extrusion off the seat base frame. This temporary extrusion was later cut out. After the fins were completed, they were attached to the seat base frame using a series of extrusions to represent the welds. These extrusions had circular and square cross sections and were cut down, whenever possible, to look more like the actual seat base. There are two short, tubular sections welded to the seat base frame under the fins. These sections are stops for the seat back; they limit the rotation of the seat back in the setup position.

4.3.3 Seat Back.

The seat back was drawn in three major steps. The long U-shaped part of the seat back is actually three pieces welded together. There are two pieces that connect to the seat base. The top piece fits snugly into the two lower pieces. The top piece was drawn first using a spline extrusion. A 3D curve was drawn, following the path of the upper piece of the seat back. The sketch was extruded along the entire length of this piece.

The two lower pieces of the seat back were drawn the same way, both using spline extrusions. Each 3D curve for the lower pieces overlapped the 3D curve for the upper piece for a few inches to represent the overlap of the frame pieces. The inner diameter of these sketches was decreased by one-half of one thousandth of an inch so the extrusion would overlap the existing extrusion by the same amount and SolidWorks would not have any tolerance problems.

There are two pins that the mounting bolts run through. Each pin was created by setting up reference geometry and extruding the cylinder. The two center cuts were made with one cut. There is a member that runs between the two lower pieces of the seat back. This piece was made by setting up a reference plane and extruding a sketch of the cross section up to surface in both directions.

4.3.4 Leg Bar.

The leg bar was drawn in three major steps. The two main members that run from the floor-mounting pegs up to the seat base-mounting brackets are different. Both members were drawn using spline extrusions. It was necessary to build a temporary base because SolidWorks 2000 does not allow disjoint components of the same part. Both members were drawn using a 3D curve followed by a sketch of the cross section extruded along the curve. There are two pins that the mounting bolts run through. Each pin was created by setting up reference geometry and extruding the cylinder. The two center cuts were made with one cut.

The connecting bar that runs between the two main leg bar members was drawn with a basic extrusion. A reference plane was set up to run parallel to the cross section and intersect the bar roughly in the middle of its length. A sketch of the cross section was then extruded up to surface on both sides, one side to one main support member and the other side to the other main support member.

The fin on the forward main support member was drawn by setting up a reference plane on the top surface of the fin. A horizontal slice of the fin would reveal the cross section used to make the sketch. The sketch was then extruded the length of the fin.

4.3.5 Stabilizer Bar.

The stabilizer bar was drawn in two major steps. First, the elbow-curved piece was drawn with a spline extrusion. A 3D curve was drawn to follow the length of the elbow-curved piece. A sketch of the cross section was extruded along the path of the curve. Second, the straight piece was drawn with a basic extrusion. No reference plane was required because plane 1 (one of

SolidWorks' basic reference geometries) could function as the sketch plane. The sketch of the cross section was extruded up to surface to the elbow-curved piece.

4.3.6 Bolts.

Each bolt was drawn with the nut and both washers in the appropriate position. The entire part was extruded radially by drawing half the cross section and extruding 360 degrees. The hex head of the bolt and the hex of the nut were added using separate cuts.

4.3.7 Pegs.

The pegs were drawn in two steps. First, the rigid part of the peg was drawn with a radial extrusion. Second, the sliding alignment cap was drawn as a separate part in SolidWorks and later assembled into a subassembly of the whole frame. The cap was radially extruded. The alignment notches on the rail side of the cap were cut out.

4.3.8 Three-Dimensional Assembly.

As shown in figure 4-10, the parts were assembled using all four main parts, six bolts, and four peg subassemblies. The assembly can be collapsed to form the storage position by removing two mates. One is between the fin on the leg bar and the notch on the stabilizer bar, and the other is between the bottom of the seat back and the stops on the seat base.

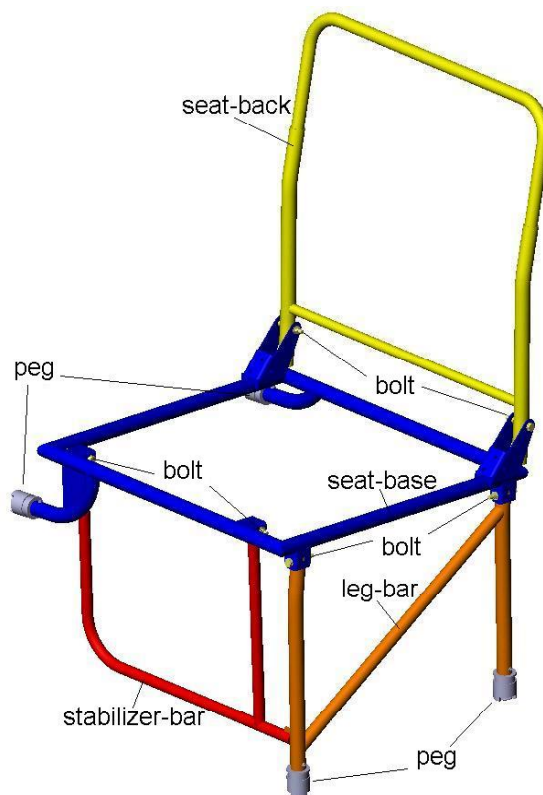


FIGURE 4-10. GEOMETRIC MODEL OF THE REFERENCE SEAT

In the setup position, the assembly can be attached to two mounting rails and a mounting base. The rails were drawn to match the Beechcraft mounting rails that the high- and low-back seats attach to. The base is just a generic wedge used for illustration purposes. The mounted assembly is used for illustration purposes to give the reader a better idea of how the seat attaches to the mounting rail and the airplane itself.

4.4 CONVERSION TO SHELL MODEL.

After initial runs using the HyperMesh meshing program, it was determined that the geometry in SolidWorks would have to be shell geometry. As described in section 5, this type of geometry is more compatible with the shell elements to be used in the LS-DYNA model.

Modification of the SolidWorks model from 3D geometry to shell geometry was accomplished by reducing all solid extrusions to shell extrusions. In the few places where disjoint geometry became a problem, the model was altered in the slightest way possible to reduce the overall effect on the outcome of the drop test simulation.

The mounting fins had to be narrowed to contact the seat base frame without a weld. A set of four small ring-shaped surfaces had to be inserted between the upper and lower pieces of the seat back to accommodate the disjoint geometry. The position of the fin on the leg bar had to be moved slightly to contact the forward main support member. The six mounting tubes that the bolts ran through had to be widened to contact the various main parts of the seat's frame.

The bolts were changed into tubes with a diameter and thickness selected to match the original bolt in terms of cross-sectional area. It was assumed that the bolts would not fail during any particular drop test. While this assumption may not be justified for airplane seats in general, past drop test results suggest that it is a good assumption for both the high- and low-back Beechcraft seats. All the bolts are in locations where bending of the bolts is not a major concern. For these two reasons, the tube bolt was not specifically designed to match the original bolt in terms of maximum shear stress or moment of inertia.

The pegs were also changed into tubes with a selected diameter and thickness. Since the drop test cannot include any possible deflections in the fuselage, the ends of the pegs will be assumed to be rigid, as discussed in section 5. Furthermore, there is no evidence that the pegs in standard Beechcraft seats fail during severe, but survivable, vertical drop test. For these reasons, the diameter and thickness of the tube pegs were selected to match the bending moment of the section of the peg assumed most likely to bend. The rigid part of the peg appears solid for the most part, so the section assumed most likely to bend was the length of the screw, beneath the mounting cap.

5. DEVELOPMENT OF THE FINITE ELEMENT MODEL.

5.1 MESH GENERATION.

Using the SolidWorks representation of the seat, the research team created a finite element mesh of the seat using the HyperMesh code. HyperMesh is an industry-standard finite element pre- and postprocessor that works seamlessly with LS-DYNA and other finite element codes. The HyperMesh FE mesh along with boundary conditions, loads, and constitutive properties was assembled into a finite element model for input to the LS-DYNA code.

5.1.1 Importing Geometric Model From SolidWorks.

SolidWorks can export/save IGES files from 3D and shell models. HyperMesh can import IGES files as surface geometry. This is the main mechanism by which the model was transported from SolidWorks to HyperMesh. The SolidWorks half of the process was easily accomplished by saving the model as an IGES file. The user should simply select the save as menu item and change the file extension to .igs. The HyperMesh process was slightly more involved and required the user to name the input (IGES) file and the translator. The user should click on the file menu (green button), highlight the import tab, select IGES.exe as the translator, and select the appropriate input file.

The user should avoid importing SolidWorks assemblies directly using only one IGES file. The mating information that SolidWorks uses to make the assembly is lost when the model is saved as an IGES file. After HyperMesh imports the IGES file, the parts are in their original, premated positions and the model looks like a jumble of parts. It is harder to move things around in HyperMesh than it is in SolidWorks and having all those parts overlapping each other can be very confusing. For this reason, the parts were imported and positioned one at a time. HyperMesh does not mate parts together; it only moves geometry. HyperMesh is more like AutoCAD, a general 3D drafting application, than SolidWorks in this sense.

5.1.2 Positioning Parts.

HyperMesh contains a tool called position, which is extremely useful in moving and positioning the components correctly. The process of positioning a component requires the creation of six temporary points called nodes. Two sets of three noncollinear nodes are required, one to define the initial position and another to define the final position. Each node in the initial set is linked to a respective node in the final set. All selected surfaces will be moved according to these nodes.

Another important tool is the rotate tool. This tool is very helpful in positioning parts that are free to rotate, such as the seat back, leg bar, and stabilizer bar. Since HyperMesh does not mate parts like SolidWorks, it was necessary to rotate the leg bar and the stabilizer bar several times in alternating succession to line up the fin with the notch.

All the parts were lined up using these two tools. First, the seat base is imported and then the frame is built around it. The finished model is shown in figure 5-1.

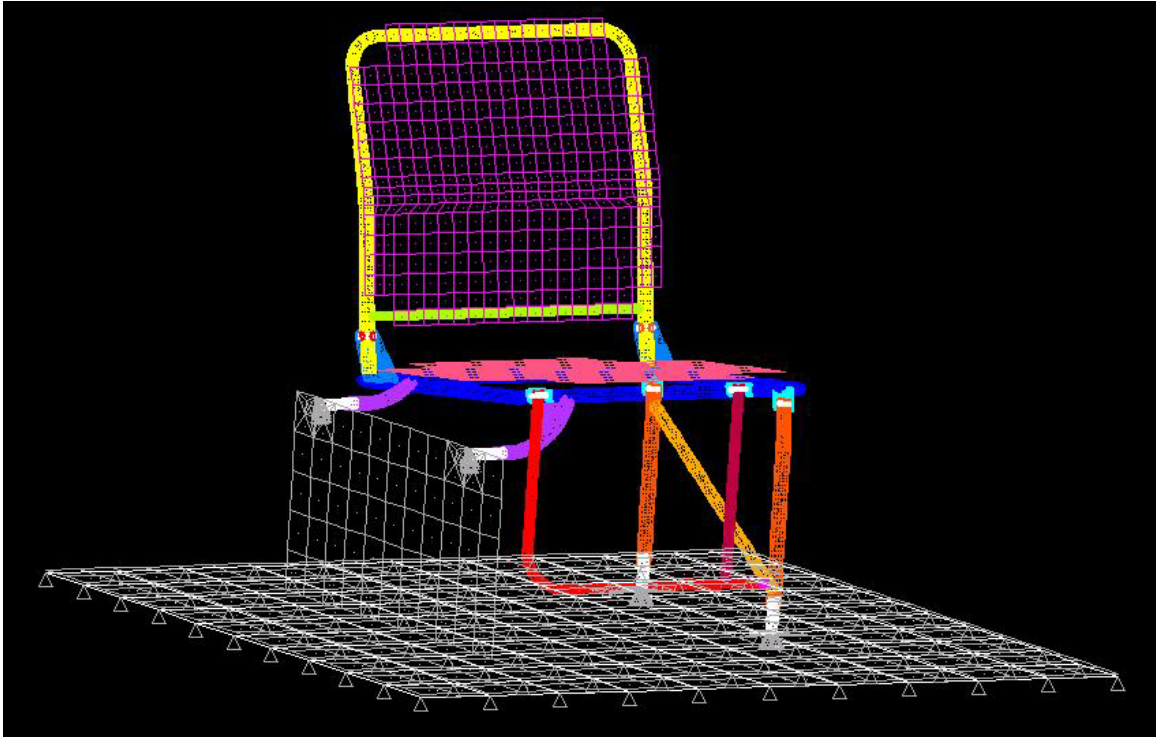


FIGURE 5-1. HYPERMESH MODEL OF THE REFERENCE SEAT

5.1.3 Collectors.

HyperMesh organizes everything in groups called collectors. A HyperMesh file may contain any number of collectors, but all things must belong to one of these groups. There are different types of collectors, such as component collectors, property collectors, and load collectors. Component collectors contain surfaces and elements, but they are separate from one another.

A separate collector was created for seat base, seat back, leg bar, stabilizer bar, each of the six bolts, and each of the four pegs. After each part was imported into HyperMesh, a component collector was created for it, and the component was assigned to that collector. Parts are assigned to collectors using the organize command.

5.1.4 Meshing.

HyperMesh offers a variety of elements and a variety of ways to create each type of element. Elements can be created automatically, in arrays, or even one at a time. Two important shell element types are the four-node quadrilateral element and the three-node triangular element. Two important solid elements are the eight-node, six-surface cube and the four-node, four-surface tetra. The eight-node, six-surface cube elements are called cubes even though they do not necessarily have to have equal sides.

The automatic mesh generation option is a powerful tool. The user can create complex meshes of shell or solid elements using these tools. Shell elements can be automatically generated by surface or group of surfaces by using the automesh command and selecting the surface(s),

element size/density, and element type (quadrilateral or triangular elements). Solid tetra elements can be created by first creating a mesh of triangulars that completely encompasses region of solid elements and then using the tetramesh command.

Most of the elements in the model were created using the automesh command. There were many places where the mesh had to be altered by hand, but, in some cases, the automesh command was sufficient in itself to build the mesh. It was important to build a mesh for each part separately so that each new set of elements could be properly organized to its respective collector. Trying to organize thousands of elements by hand would be very time consuming.

5.1.5 Solid Elements.

Originally, the model using solid elements was chosen to be built. Cube elements would be used whenever possible and tetra elements would be used otherwise. However, early in the project it was found that a solid element model would require many more elements required than a personal computer (PC) could reasonably handle.

There are a few reasons that the number of solid elements would be so high. As stated earlier, it was assumed that most of the large deformations in the frame would look more like a beam in bending and less like a rod in tension or compression. In a finite element model, it is necessary for a component to have a minimum thickness of three solid elements to describe bending with any level of accuracy. The thickness of the seat frame tube structure is very thin, in some places less than forty thousandth of an inch. These tube walls would drive the required element size down to the range of ten thousandths of an inch. The resulting number of elements to represent a 6-inch length of frame would be on the order of 200,000.

In LS-DYNA, the basic solid elements are cubes and tetrahedrons. Nodes connected to solid elements have three degrees of freedom; they may translate in the x, y, and z directions. Nodes connected to shell elements, however, like quadrilaterals and triangulars, have six degrees of freedom. Shell elements can translate, but can also rotate about three axes. This inherent characteristic of shell elements makes them a much better choice to describe bending than solid elements.

5.1.6 Shell Elements.

Since most of the geometry is thin and of constant thickness, shell elements was the next element for consideration. Shell elements typically require an aspect ratio of ten to one to get any accuracy in the result. The seat frame exhibits a larger aspect ratio almost everywhere except for the tips of the fins around the bolt holes, where the aspect ratio is closer to six to one. Fortunately, that section of the frame does not appear to be particularly susceptible to bending in a vertical drop test because of its vertical orientation.

Nodes in HyperMesh have six degrees of freedom. Unlike solid elements, shell elements make use of all six axes. Therefore, a shell element not only takes into consideration the x, y, and z position of each of its nodes, but also the rotation about each axis. This means that HyperMesh shell elements do not have to be planar; they can be curved to fit the side of a cylinder or any

other surface. It also means that there is a built-in bending calculation already going on inside each shell element.

The number of shell elements in the same six-inch section of tubular member becomes closer to 700. Taking all this into consideration, it was decided that shell elements would be an acceptable alternative to solid elements.

The surfaces of the original model were constructed using solid elements. To make the finite element model out of shell elements, the surfaces had to be modified accordingly in SolidWorks. Once the conversion to shell elements was completed in SolidWorks, the process of importing and positioning surfaces described above was repeated.

5.2 DEVELOPMENT OF THE LS-DYNA MODEL.

LS-DYNA is a general-purpose, explicit finite element program used to analyze the nonlinear dynamic response of 3D structures. The code is used extensively to model the response of passenger vehicles and occupants to crash loading. LS-DYNA has unique solution procedures that allow the code to simulate the physical behavior of 3D structures: nonlinear dynamics, thermal, failure, crack propagation, contact, quasi-static, Eulerian, ALE, fluid structure interaction, real-time acoustics, and multiphysics coupling.

As described below, the to develop the LS-DYNA model combined the HyperMesh mesh with boundary conditions, initial conditions, contact interfaces, and constitutive properties.

5.2.1 Keywords and Cards.

LS-DYNA reads and compiles input from a single file and records output in at least five different files. It can be set to output other types of files if specified in the input file. All the commands that LS-DYNA recognizes are called keywords. A keyword is preceded by an asterisk in the input file. The keyword part, for instance, would appear as *part in the input file. Each keyword has one or more associated cards. The cards contain information that the keyword uses to carry out a command. The keywords can be thought of as functions, and the cards can be thought of as the input variables of the function. The cards are just an organization of the variables and are nothing more than a row of variables. LS-DYNA holds up to eight values in one card (row). If a keyword requires more than eight variables, it may require more than one card.

5.2.2 Setup With HyperMesh.

The LS-DYNA package comes with a preprocessor, Ingrid, and a postprocessor, Post-GL. Ingrid is much less powerful and much harder to use than HyperMesh. HyperMesh is fully compatible with LS-DYNA and can effectively function as model builder and a preprocessor.

There is an option in HyperMesh to declare a template file. The purpose of the template file is to set the HyperMesh environment to be compatible with the respective simulator. By setting the template file to dyna.key, HyperMesh becomes completely compatible with LS-DYNA.

HyperMesh can export LS-DYNA input files. To make use of this feature, the user should click on the file menu, highlight the export tab, select dyna.key as the template file, and select the appropriate LS-DYNA input file name. Although not required, the user should add the extension .dyn to LS-DYNA input files for organization.

HyperMesh will automatically include some information, like node data and element data. Other information is included: property collector data, organized under the *section keyword, and material data is included under the *material keyword. However, this information will not be correct unless it is set up correctly in HyperMesh. Finally, there are a number of keywords that will not be included unless specified. Many of the *control family keywords fall into this category, like *control_termination and *control_contact.

5.2.3 Simulation.

Once a model has been completed in HyperMesh and a .dyn file has been created, LS-DYNA can run a simulation. To run a simulation, open the LS-DYNA manager, go to run setup. If LS-DYNA fails to compile the .dyn file, the .dyn file most likely contains errors or warnings. Any error results in an error termination message, which means that LS-DYNA failed to compile the input file. It is possible for LS-DYNA to compile and run a .dyn file that produces warnings without errors, but these warnings should not be taken lightly. Most of the warnings are particularly serious and very few simulations that contain warnings produce meaningful results, even if they compile correctly. Since simulation times may be large, it may not be counter-productive to ignore warnings.

As soon as LS-DYNA has compiled a .dyn file, it begins the process of computing the dynamic solution to the finite element model. In the last few lines before the time output information, there will be the estimated run time. This time is not always accurate. If there is a spike in the PC processor usage from another program, like explorer, at the same instant that LS-DYNA computes the estimated run time, the value of the run time will be much higher than it should be. If the estimate run time is extraordinarily high, it may be necessary to restart the simulation to obtain a more accurate estimate of run time.

5.2.4 Postprocessing.

Post-GL is the LS-DYNA's postprocessor. Post-GL is capable of reading LS-DYNA's main output file (3Dplot) and building a four-dimensional (multiple time point, 3D plot) graph file or video clip. During a simulation, LS-DYNA records the nodal positions, elemental stresses, and deformation at preset time intervals. Post-GL reads this data and transforms it into a set of graphs for each time interval. At any particular time interval, the user can view the elemental stresses, strains, displacements, and many other items of interest. Post-GL color-codes the graph with up to 25 different shades, each representing a different range of values.

Post-GL can string all or some of the graph of a single type, e.g., stresses, together to create a video clip of the simulation. It can show from beginning to end how the stresses change in the model. Any single viewpoint can then be chosen to build a video clip from. Post-GL can build .avi files by clicking on the .avi icon at the top left-hand side of the screen.

Postprocessing is an invaluable part of modeling. After suitable output is obtained, either in the form of a video clip, resultant values, or insight into the model, the next step is to go back to the HyperMesh model and alter it to obtain an even better result. A typical simulation result is shown in figure 5-2.

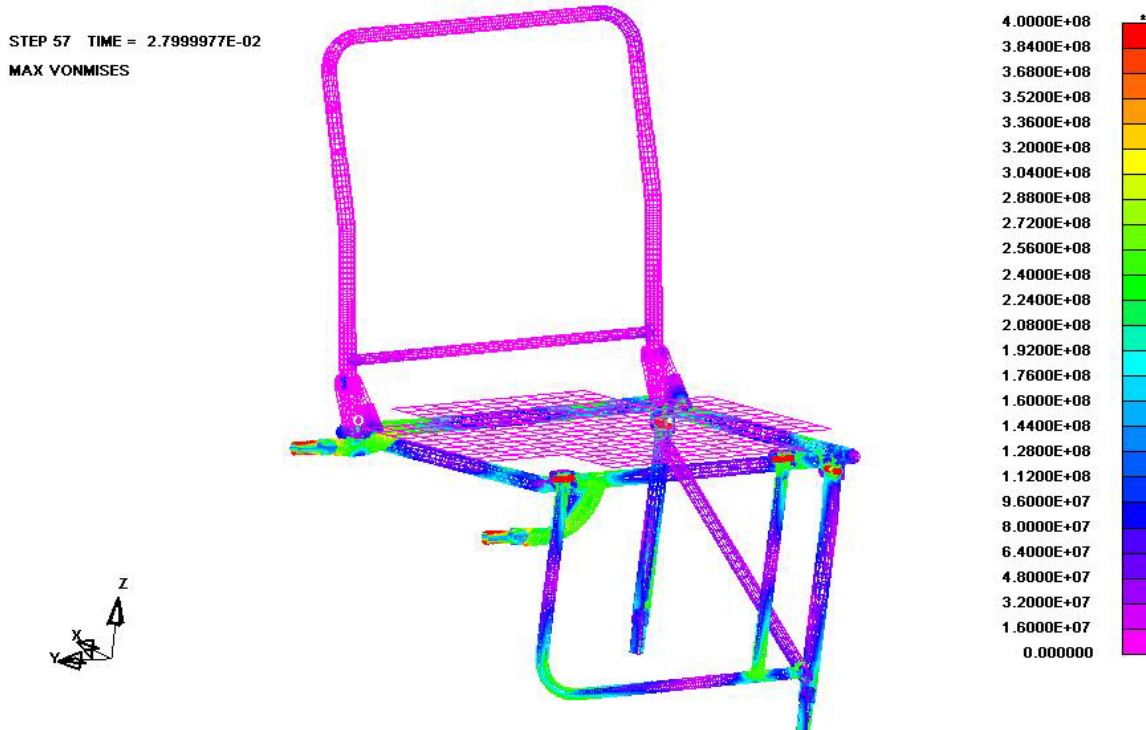


FIGURE 5-2. LS-DYNA MODEL OF REFERENCE SEAT SHOWING STRESSES IN A TRIAL RUN

5.2.5 Loading Conditions.

The model of the reference seat was loaded in two different ways: (1) the velocity drop test and (2) the acceleration base test. The velocity drop test was used to simulate drop tests in the Rowan Drop Tower. The acceleration-base test was used to simulate full-scale fuselage drop tests conducted by the FAA. Both types of simulations were conducted to validate the model against experimental data.

In the velocity drop test, the model is subjected to a prescribed impact velocity. In this test, the seat is attached to a drop frame. The drop frame closely resembles the drop frame used in the FAA full-scale fuselage drop test. The system is given an initial velocity and bounded by a rigid wall. The rigid wall functions as the concrete base in the actual drop test. This drop test most closely resembles the actual drop test in terms of visual and physical comparability.

In the acceleration base test, the model is subjected to prescribed acceleration versus time or crash pulse. From FAA test reports, the crash pulse was obtained using the seat track acceleration determined in the test. In the actual test, it is this acceleration with which the seat/dummy assembly is actually loaded. To model an acceleration base test in LS-DYNA, the

drop frame and rigid wall of the velocity drop simulation were removed. In their place, nodal accelerations are applied to the ends of the mounting pegs where the seat would attach to the drop frame. The accelerations can then be made to follow any chosen load curve, including the measured data from previous FAA drop tests and Rowan University drop tests.

These two loading conditions produced different results. The reason was that the velocity drop test intrinsically provides its own load curve at the mounting pegs. If the velocity drop test is run and the accelerations at the mounting peg end nodes are recorded, it can be used as the load curve in the acceleration base test. Doing this provides results that match very closely.

The velocity drop simulation was used to validate the model against results from the Rowan drop tower. The acceleration base simulation was used to validate the model against the FAA drop test of a full-scale Beechcraft 1900C fuselage.

5.2.6 Boundary Conditions.

In the velocity drop test, the only boundary condition is the rigid wall. All parts, even the drop frame, are assumed to have some elastic or elasto-plastic material properties. Parts that are assumed not to fail are typically made elastic. In the acceleration base tests, the acceleration-loaded nodes are bounded so they only translate in the z direction. This erases the tendency of the seat to rotate, due to uneven loading. No further boundary conditions are necessary.

5.2.7 Initial Conditions.

In the velocity drop test, the entire system is given some initial velocity. Kinematics is used to determine the impact velocity of a 1-, 1.5-, and 2-meter drop test. In this test, some amount of energy is added to the system initially and absorbed by the rigid wall and various members during the simulation. In the acceleration base test, the loaded nodes are accelerated in the positive z direction (upward). The magnitude of the acceleration follows a prescribed curve. In this type of test, there is initially no energy in the system. Energy is added through the loaded nodes and absorbed by the various members of the seat and dummy.

5.2.8 Contacts.

When it is known that two parts of the model will need to interact with each other, it is necessary to add a contact interface into the model. In most cases, a surface-to-surface contact type is used, but a few contacts use the nodes-to-surface type. All the vector normals (positive normal vector of each element) must be checked to ensure that contacting elements are pointing towards each other. If not, LS-DYNA should automatically reverse such contacts, but the user should not assume that this is guaranteed. If not, some nodes may be on the wrong side of the contact interface. This error can be devastating to a model. The symptoms can include wild deformations, shooting nodes, or in extreme cases, may even crash the simulation.

LS-DYNA handles contacts by placing forces on nodes that have penetrated a particular surface. This force is scaled by the distance that the node has penetrated the surface. If the value of the force becomes too large, the node will be set free and no longer be part of the contact interface. If freed nodes are unacceptable, the contact interface must be changed or the time step scale

factor can be reduced. It is possible for fast moving objects to step over a contact surface. In this scenario, the time step is way too large for the simulation, and the object nodes are set free only a few cycles after they contact the surface. The object appears to simply pass through the contact surface.

5.2.9 Element Formulation.

The default shell element in LS-DYNA is the Belytschko-Tsay Type 2 shell. This formulation is very fast, but it can produce a phenomenon called hourglassing. When hourglassing occurs, it is due to a mathematical shortcut in the shell integration process. If a simulation creates errors or produces bad results with element formulation Shell Type 2 (the Belytschko-Tsay formulation), it is suggested that the modeler use a different type of element. For example, the fully integrated shell element formulation (Shell Type 16) totally eliminated hourglassing.

5.2.10 Material Types.

All of the components of the seat frame have been given the properties of steel. Parts assumed not to fail have been made elastic, while failure and deforming parts are made elasto-plastic with failure (material type 24 piecewise linear plasticity). The seat pan and seat back pan both use element type 34 (fabric). The dummy is made with a customized elastic material so that modulus and density can be scaled to closely match the properties and weight of a crash test dummy.

5.2.11 Control Cards.

The model is set up so that shell thickness is taken into account at contact interfaces. The LS-DYNA default is that the contact happens at the center of the shell, or as it appears in the preprocessor. Using shell thickness is more realistic. However, if the modeler does not plan to use this option from the beginning of the model construction, the model could have problems with initial penetrations. Generally, it is acceptable to disregard shell thickness.

The standard time step scaling factor, a factor LS-DYNA uses to reduce the time step size to a safe size, of 0.9 is used. The simulation time is typically set for 100 milliseconds. Three-dimensional plots are typically exported every millisecond for an effective sampling rate of 1 kHz. To avoid aliasing problems however, selected nodal and elemental data were exported at a much faster sampling rate of 500 kHz. Depending on the exact conditions set forth by the finite element model, sometimes aliasing seemed to begin at sampling rates between 100 kHz and 1 MHz. Graphs that exhibited any degree of aliasing at 500 kHz were rejected.

5.2.12 Modeling the Dummy.

To determine the crash loads on a passenger located in the reference seat, a combined seat and crash test dummy finite element model was developed. As shown in figure 5-3, an 8000-element crash test dummy HyperMesh model had been successfully integrated with the Beechcraft seat model. The incorporation of the dummy model into the system will facilitate more realistic impact loading of the seat structure.

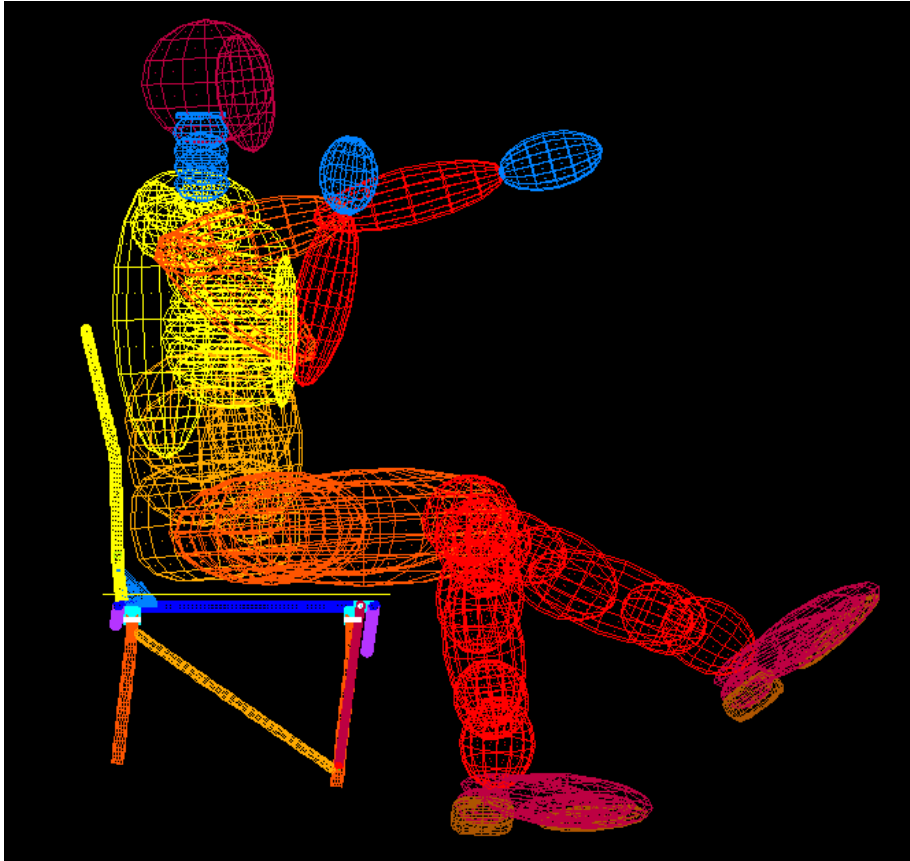


FIGURE 5-3. BEEHCRAFT SEAT MODEL WITH THE DUMMY FE MODEL

5.2.13 Constitutive Properties for Seat Model.

The geometry of the model was developed by a complete teardown and measurement of the reference seat. The seat frame is composed of high-strength steel. The seat cushion is composed of a foam covered by a loosely woven fabric. The constitutive properties of these materials for input to the model were obtained from standard tabulations of material properties. Constitutive properties are listed in table 5-1.

TABLE 5-1. CONSTITUTIVE PROPERTIES

Material	Young's Modulus	Yield Stress	Ultimate Stress	Material Behavior
Steel	200	290	476	Elasto-plastic with strain-rate effects and failure
Fabric	100	none	none	Elastic-fabric with rigidity

5.2.14 Minimizing Simulation Run Times.

Depending on the complexity of the model, the LS-DYNA simulations sometimes ran as long as 7 days. LS-DYNA run times can be greatly reduced using a number of techniques listed below:

- Almost all the LS-DYNA default settings are designed for maximum speed. The user should not change things like the time step scaling factor or the element formulation unless absolutely necessary.
- When using contact interfaces, it is a good idea to use contact component reductions. If contact is to take place between a relatively small component and a much larger component, the solver will need to check every element from each component for penetration. If one only includes elements that are likely to contact, you can drastically decrease simulation time.
- Before running a simulation, a number of checks should be performed to ensure that the simulation has no orientation errors. Running a penetration check will reveal any initial penetrations and help to eliminate errors due to initially moved nodes.
- A time step check is key to reducing simulation times. Each element has a fundamental minimum time step associated with it. LS-DYNA checks every element and every iteration to determine the element with the smallest time step. This smallest value is then scaled by the time step scaling factor to find the time step for that particular iteration. A time step check can be run in the preprocessor stage to determine which elements will initially control the time step. If these limiting elements are somehow altered to increase the size of their fundamental time steps, then the speed of the simulation can be increased dramatically. Even well constructed models sometimes contain such elements, which reduce the overall time step by a factor of 2, 10, or even 100. Altering or eliminating such elements will increase simulation speed.
- The fundamental time step, for each element, is a function of the modulus (E), the density, the size, and dimensions of the element. The time step can be increased by reducing the modulus, increasing the density, increasing the size of the element, or reducing the warpage or the aspect ratio of the element. A technique called mass scaling is sometimes useful. In mass scaling, the density of the few limiting elements is increased until these elements no longer limit the entire simulation. Typically, these elements will be very small, so the additional mass is negligible. Because this technique will introduce some amount of error however, some modelers try their best to avoid using mass scaling.
- Wherever possible, rigid elements should replace deformable elements. Making an element rigid eliminates more than 90% of the mathematical operations required during a simulation. If many components can be assumed rigid, the simulation time can be dramatically decreased.

- Drop tests should be transformed into impact tests by using kinematics. Replacing gravity and height by an initial velocity can reduce ultimate simulation times by incredible amounts. The relatively long time it takes for the contact entity to accelerate and make contact with the contact surface will account for the major portion of the total simulation time, typically more than 90%.

By making such changes, it is possible to turn simulation hours into simulation minutes. Optimizing a simulation can be very time-consuming; however, in almost all cases, the time spent during optimization will pay for itself after one or two simulations.

6. DROP TOWER TESTING.

This section presents the results of a parallel experimental program, conducted to validate the model, in which instrumented crash dummies were drop tested in the reference seat at the same impact velocities as the simulation.

6.1 OVERVIEW OF THE ROWAN UNIVERSITY DROP TEST FACILITY.

In 1998, Rowan University began a research collaboration with the FAA William J. Hughes Technical Center to investigate aircraft crashworthiness in severe but survivable crashes. One result of this research was the development of an 18-foot drop tower capable of simulating lower severity aircraft crashes. A drawing of the drop tower is shown in figure 6-1.

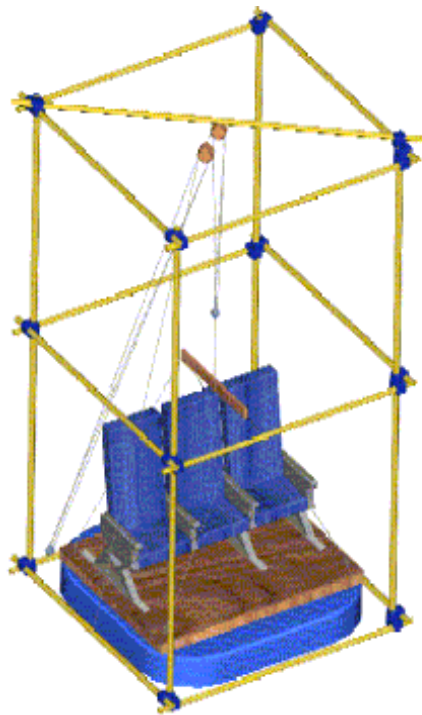


FIGURE 6-1. THE ROWAN UNIVERSITY DROP TOWER

The drop tower has been successfully used to evaluate the crash energy-absorption capability of aircraft seats used in commuter category aircraft, e.g., the Beechcraft 1900C. In these tests, an instrumented crash test dummy in the seat is hoisted to the desired height and allowed to drop in free-fall onto an impact block at the base of the tower. The dummy is instrumented with sensors that include an accelerometer in the pelvis and a six-axis load cell in the lumbar spine. The seat and seat fixture platform are instrumented with accelerometers to record structural impact loadings. The impact block can be rigid or designed to mimic the structural force deflection of the underlying aircraft structure. A pretest photograph of an aircraft seat with seated crash dummy is shown in figure 6-2.



FIGURE 6-2. INSTRUMENTED CRASH TEST DUMMY SEATED IN THE ROWAN UNIVERSITY DROP TOWER

6.2 DESCRIPTION OF THE DROP TOWER.

The drop tower apparatus is composed of several components: the drop tower structure, the seat platform fixture, the hoist/quick release mechanism, and the impact block.

6.2.1 Drop Tower.

The drop tower is constructed of heavy steel scaffolding approximately 18 feet in height. A block and tackle system is used to hoist the test article to the desired height. One pulley is attached to the middle of a single hollow steel tube that is fixed diagonally across the top. A second pulley is attached to the top of the seat platform. The block and tackle system is threaded with high-strength metal cable. One end of the cable is terminated on the upper pulley while the other end of the cable is attached to a winch, as shown in figure 6-1.

6.2.2 Seat Platform.

The seat is attached to the seat platform fixture shown in figure 6-3. The platform fixture is constructed of 1" hollow-square aluminum tube with a 1/8" thick aluminum plate bolted to the top and bottom. In a test, the seat platform fixture with attached seat and dummy was hoisted to the desired height and dropped in free-fall onto the impact block. Mounted to this platform are a floor rail and a side rail that accepts a Beechcraft 1900C aircraft seat. The platform was designed to be rigid and durable. The platform will be

used for many impact tests and must be able to withstand extreme forces without significant deformation. In addition, the platform must be sufficiently rigid to prevent excessive residual vibrations during either free-fall or impact. Both the finite element model and the analysis of the test results will assume a rigid, i.e., nondeformable, platform.

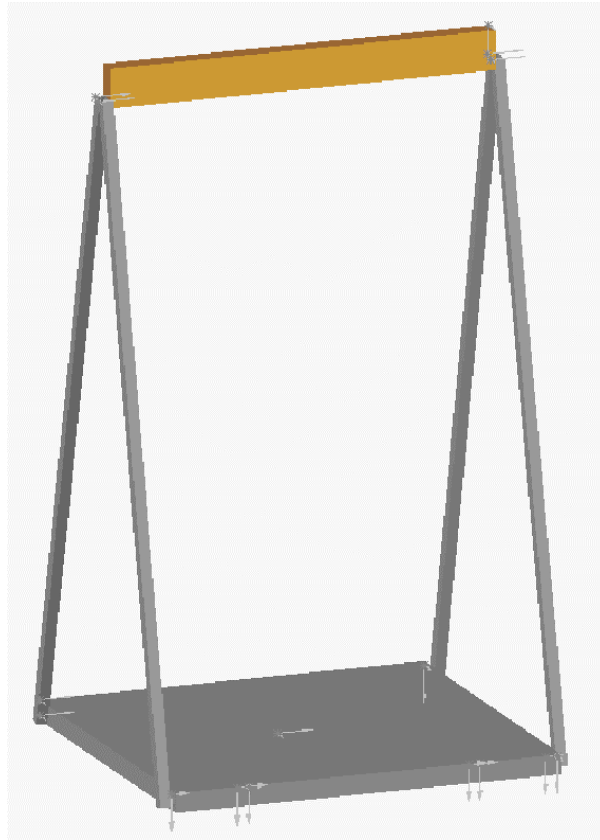
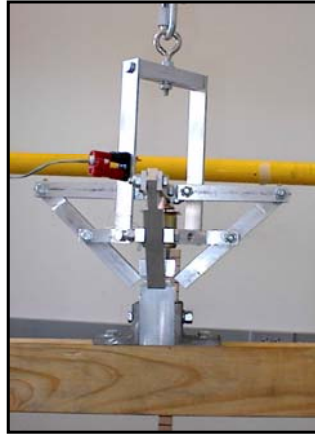


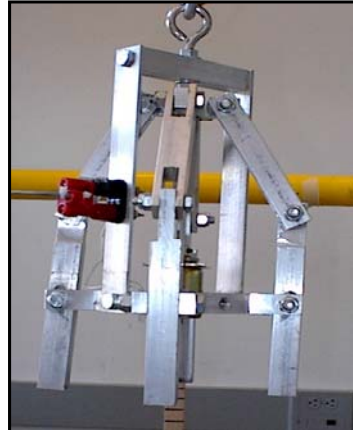
FIGURE 6-3. SEAT PLATFORM FIXTURE

6.2.3 Hoist and Quick Release Mechanism.

As shown in figure 6-4, a unique hoist and quick release mechanism was designed and fabricated for this project to raise and drop the platform. The mechanism was designed to release the seat assembly in free-fall without introducing any spurious horizontal motion. To hoist the seat assembly, one end of a cable is attached to a manual winch and pulled through a block and tackle pulley arrangement with the release mechanism attached to the lower block pulley. The mechanism is a series of four bar linkages that grasps onto a grooved aluminum block that is connected to the seat platform by means of belts and bars. In the gripping position, the mechanism holds firmly yet is just resting below a toggle point. Once the platform has been lifted, a solenoid mounted in the center of the mechanism is responsible for nudging the linkage assembly through a toggle point, thereby allowing the platform to free-fall.



(a) Closed



(b) Open

FIGURE 6-4. HOIST AND QUICK RELEASE MECHANISM

6.2.4 Impact Block.

The purpose of the drop tower test is to gather data on the effects that a shock impact would have on a human seated in an aircraft seat. One factor that controls the level of shock that the dummy will undergo is the type of surface on which the seat assembly lands. Early checkout tests of the drop tower dropped the seat assembly on four truck tires. These tires dampened the landing and therefore decreased the maximum shock seen by the dummy. The finite element model, however, assumes that the impact surface is rigid. A rigid impact surface will subject the seat and dummy assembly to high-G impacts from relatively low altitude drops. In addition, a rigid impact surface can be easily modeled.

For this project, the research team constructed a 5' x 5' x 4" deep fiber-reinforced concrete impact block inside the drop tower footprint. Professor Douglas Cleary, a Rowan University Civil Engineering professor, designed a high-strength concrete mix for the impact block which would be inexpensive, have high resistance to damage, and would be straightforward to replace in case of failure. Figure 6-5 shows the completed impact block.



FIGURE 6-5. IMPACT BLOCK FOR ROWAN UNIVERSITY DROP TOWER

During construction of the impact block, samples were drawn from the concrete mix to create 4" diameter concrete cylinders. These cylinders, after a 28-day curing period, were used to determine the strength of the impact block. The cylinders were capped and tested as per American Society for Testing and Materials specification C 617 and C 39, respectively, and were able to endure a maximum load of 72,495 pounds, corresponding to a maximum yield compressive strength of 6,000 pounds per square inch (psi). By comparison, ordinary sidewalk concrete can sustain 3000 psi, while structural concrete ranges from 4000 to 6000 psi. Higher-strength concrete mixtures that can sustain 8000 psi are used in special applications such as skyscrapers.

6.3 TEST ITEMS.

6.3.1 Anthropomorphic Test Device.

The anthropomorphic test device used in the drop tests was a Hybrid II 50th percentile male dummy with an FAA modification—a load cell implanted in the lower lumbar. The dummy, shown in figure 6-6, was loaned to the research team by the FAA William J. Hughes Technical Center. When calibrated, the Hybrid II dummy is designed to provide realistic characteristics with respect to the human range of motion, response to forces, center of mass, and distribution of mass. However, the dummy used in this program has not been calibrated by the FAA in many years and was noticeably stiff in its joints.



FIGURE 6-6. HYBRID II CRASH TEST DUMMY

6.3.2 Surrogate Test Seat.

Before conducting the drop tests with the Beechcraft 1900C seats, a methodical checkout of all components of the drop test facility was performed. The checkout included over a dozen full dress rehearsal trial drop tests. To avoid using any seats from the limited supply of Beechcraft 1900C seats, a surrogate seat for system checkout and trial drop tests was needed.

Because numerous checkout tests were anticipated and each test would destroy a chair, the cost per chair was the controlling factor in choosing a surrogate chair. After considering many alternatives, including fabricating the chairs, the most economical surrogate was found to be ordinary lawn chairs. The chairs are inexpensive and can be easily attached to the seat platform with U-bolts. Figure 6-7 shows a surrogate seat.



FIGURE 6-7. SURROGATE SEAT FOR DROP TOWER CHECKOUT TESTS

Seven lawn chairs were initially purchased from a local discount store for under \$10 each. After running numerous tests, an additional ten chairs were purchased for roughly the same price. Using these surrogate seats, checkout tests were run without worrying about one of the components not properly working. Note that these surrogate seats were only used during system setup and checkout. The surrogate chairs were not used in any way to validate the finite element model.

6.3.3 Instrumentation.

The Hybrid II crash test dummy had been thoroughly instrumented by the FAA William J. Hughes Technical Center, as shown in table 6-1. The chest and the head were each instrumented with three Endevco 7231C-750 single-axis accelerometers aligned along the x, y, and z axis. The pelvis was instrumented with an Endevco 7231C-750 single-axis accelerometer aligned along with the z axis. Only a single accelerometer could be installed in the pelvis, because of lack of space. The FAA has calibrated all the accelerometers. Each accelerometer uses a supply voltage of 10 volts.

TABLE 6-1. DROP TEST INSTRUMENTATION (SENSORS)

Channel Number	Sensor Attachment	Measurement	Orientation	Transducer	Sensitivity	Units	Full-scale Range \pm	Units
1	Head	Acceleration	x axis	Endevco 7231C-750	0.1973	mV/g	750	G's
2	Head	Acceleration	y axis	Endevco 7231C-750	0.2292	mV/g	750	G's
3	Head	Acceleration	z axis	Endevco 7231C-750	0.1890	mV/g	750	G's
4	Chest	Acceleration	x axis	Endevco 7231C-750	0.1973	mV/g	750	G's
5	Chest	Acceleration	y axis	Endevco 7231C-750	0.2005	mV/g	750	G's
6	Chest	Acceleration	z axis	Endevco 7231C-750	0.2021	mV/g	750	G's
7	Pelvis	Acceleration	z axis	Endevco 7231C-750	0.1966	mV/g	750	G's
8	Platform	Acceleration	z axis	Endevco 7231C-750	0.2	mV/g	750	G's
9	Lower Lumbar	Force	x axis	R. Denton 1708	0.004127	mV/lbs	3000	lbs
10	Lower Lumbar	Force	y axis	R. Denton 1708	0.004120	mV/lbs	3000	lbs
11	Lower Lumbar	Force	z axis	R. Denton 1708	0.001694	mV/lbs	5000	lbs
12	Lower Lumbar	Moment	x axis	R. Denton 1708	0.001813	mV/in-lbs	10,000	in-lbs
13	Lower Lumbar	Moment	y axis	R. Denton 1708	0.001823	mV/in-lbs	10,000	in-lbs
14	Lower Lumbar	Moment	z axis	R. Denton 1708	0.002783	mV/in-lbs	4000	in-lbs

The lower lumbar of the test dummy was instrumented with an R. Denton Model 1708 load cell, as was done with the previous dummy. The load cell that was used was a six-channel load cell, three channels for axis forces and three channels for moments about each axis. With a 10-volt excitation, its sensitivity is given as 0.001694 mV/lbs.

The tests also measured the seat platform acceleration. When integrated, this channel provides a check on the impact velocity that the seat/dummy combination experiences. The platform was instrumented with an Endevco 7231C-750 accelerometer located on the left-hand side of the seat platform fixture.

6.3.4 Data Acquisition Systems.

The data acquisition system (DAQ) is a National Instruments SCXI-1000 system, coupled with a National Instruments PCI-MIO-16E-1 analog-to-digital (A/D) board. The SCXI-1000 system provides signal conditioning, while the PCI-MIO-16E-1 provides high-speed A/D conversion of the analog inputs. A custom software program, written using LabView, controls the entire system.

The SCXI-1000 is a four-slot chassis that can house up to four SCXI modules. This research program used two SCXI-1520 eight-channel Universal Strain/Bridge modules to provide signal conditioning for up to 16 piezoresistive accelerometers or load cells. Each SCXI-1520 module can accept eight channels. Each channel has a separately programmable gain, excitation, and anti-aliasing filter. The unit provides automatic null compensation in hardware. Although the instruments use a full bridge, the SCXI-1520 provides quarter-, half-, or full-bridge completion modules for use with other instruments such as strain gages. The SCXI-1520 also provides two independent shunt-calibration circuits per channel. Each SCXI-1520 was equipped with an SCXI-1314 Front-Mounting Terminal Block for cable connection.

The system used a National Instruments PCI-MIO-16E-1 card mounted in a PC to perform A/D conversion. A 6-foot shielded cable connects the SCXI and the A/D card. The PCI-MIO-16E-1 can perform 12-bit A/D at a sampling rate of 1.25 MHz. The card can either accept 8 double-ended or 16 single-ended analog inputs. For these tests, the sampling rate was set at 20,000 samples per second per channel. Only one channel of the PCI-MIO-16E-1 was used. The analog inputs in this system were multiplexed to the A/D board by the SCXI-1000 signal-conditioning system.

6.3.5 Kodak MotionCorder.

An important component in this setup was the Kodak MotionCorder. A high-speed digital camera, shown in figure 6-8, can achieve a frame rate of up to 600 frames per second (fps). The frame rate is adjustable and can be set at 30, 60, 120, 240, 400, and 600 fps. The camera contains random access memory that stores the digital video temporarily. The camera can playback the video at variable frame rates as well (as low as 2 fps up to 600 fps).



FIGURE 6-8. KODAK MOTIONCORDER HIGH-SPEED DIGITAL VIDEO RECORDER

In this application, the camera was manually triggered at the same time as the DAQ system. The camera was set up with the trigger as its center point. In other words, the camera was continuously recording and took the same amount of video before and after the trigger was activated. This gave an outstanding video of the seat in free-fall and at impact. From this video, it was determined how the seat failed and the impact velocity of the platform.

6.4 RESULTS.

This section presents the results of a parallel experimental program, conducted to validate the model, in which instrumented crash dummies were drop tested in the reference seat at the same impact velocities as the simulation. As shown in table 6-2, drop tests were conducted from nominal heights of 1, 1.5, and 3 meters onto a rigid surface.

TABLE 6-2. DROP TEST MATRIX

Test Number	Test Date	Target Drop Height (meters)	Actual Drop Height (meters)	Target Impact Velocity (m/s)
2003-01-10-1m	01-10-2003	1	1	4.4
2003-01-17	01-17-2003	1.5	1.5	5.4
2003-01-10-2m	01-10-2003	2	2	6.2

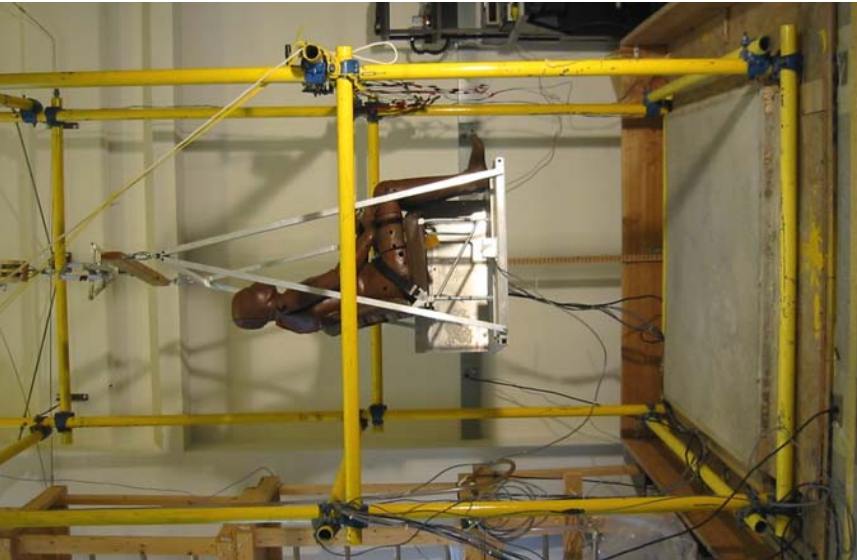
As shown in appendices A, B, and C, the actual drop height was measured immediately before each test. The target impact velocities in table 6-2 were computed from kinematics. Neither velocity was measured. Table 6-3 presents a summary of the impact test results for each channel. More detailed reports for each report are included in appendices A, B, and C. Figure 6-9 presents pretest photographs of each drop test. The appendices present posttest photographs of each test as well as closeup photographs showing points of seat failure.

TABLE 6-3. DROP TEST PEAK MEASUREMENTS—ABSOLUTE VALUE

Channel Number	Sensor Attachment	Measurement	Orientation	Filter (Hz)	1-m drop	1.5-m drop	2-m drop	Units
1	Head	Acceleration	x axis	1000	7.4	60.3	38.9	G's
2	Head	Acceleration	y axis	1000	6.1	36.0	29.3	G's
3	Head	Acceleration	z axis	1000	28.7	56.9	87.5	G's
4	Chest	Acceleration	x axis	180	0.1	0.6	1.0	G's
5	Chest	Acceleration	y axis	180	8.8	-	-	G's
6	Chest	Acceleration	z axis	180	23.8	38.9	57.4	G's
7	Pelvis	Acceleration	z axis	180	21.3	68.2	80.8	G's
8	Platform	Acceleration	z axis	60	172.2	-	-	G's
9	Lower Lumbar	Force	x axis	60	218.8	-	-	lbs
10	Lower Lumbar	Force	y axis	60	122.2	-	-	lbs
11	Lower Lumbar	Force	z axis	60	1157.6	-	-	lbs
12	Lower Lumbar	Moment	x axis	60	367.0	254.1	372.9	in-lbs
13	Lower Lumbar	Moment	y axis	60	517.1	1204.7	1206.8	in-lbs
14	Lower Lumbar	Moment	z axis	60	58.9	52.2	66.0	in-lbs

Notes:

1. The lower lumbar axial and shear load cell channels failed during both the 1.5- and 2-m tests. The lower lumbar moments however were successfully measured. The platform accelerometer channel also failed during these two tests. The chest y axis accelerometer was measured, but the data was of questionable accuracy. The appendices contain plots of all channels, including those described in this note.
2. Maximum values shown in this table are absolute values.



(a) 1-meter drop test



(b) 1.5-meter drop test



(c) 2-meter drop test

FIGURE 6-9. SEAT AND DUMMY ASSEMBLY AT DROP HEIGHTS JUST PRIOR TO DROP TESTING

7. IMPACT SIMULATIONS.

The model was validated against the results of a series of three drop tests conducted at the Rowan University drop tower. In each drop test, an instrumented Hybrid-II dummy was seated in a Beechcraft 1900C seat, raised to the desired drop height, and released in free-fall to impact on a hardened concrete block. The Beechcraft 1900C seat was dropped onto a rigid impact surface from heights of 1.0, 1.5, and 2 meters. The seat was replaced between each test.

To validate the finite element model, a simulated drop test was conducted using the same drop heights as the three physical experiments. The results of the computer simulation were compared with the experimentally measured results of the physical experiment. Ideally, the computer simulation should agree with the physical experiments. It should be noted that unlike many modeling efforts, which tune the model to match the experiment evidence, the program completed model development several months before the experiments were completed. Thus, there was no opportunity for model tweaking. The excellent agreement between model and experiment described below is the direct result of a committed effort early in this project to capture the seat characteristics with unusual fidelity.

7.1 APPROACH.

Each experiment and corresponding experiment were compared by overlaying and comparing time history of critical parameters against each other. For this study, the experimentally measured and computationally simulated pelvic acceleration and axial lumbar load were compared.

7.2 COMPARISON OF SIMULATED DROP TESTS WITH EXPERIMENTAL RESULTS.

There was excellent agreement between the simulation and the experiment for the 1-meter drop test (figures 7-1 and 7-2) both in terms of peak measurement and time of peak. Figures 7-3 through 7-4 compare the simulation and experimental results from a 1.5-meter drop test. Because the lumbar force transducer failed in this test, figure 7-4 contains a plot of computational results only. Figures 7-5 and 7-6 compare the simulation and experimental results from a 2-meter drop test. Because the lumbar force transducer failed in this test, figure 7-6 contains a plot of computational results only. A complete set of experimental results and test photographs are contained in the appendices.

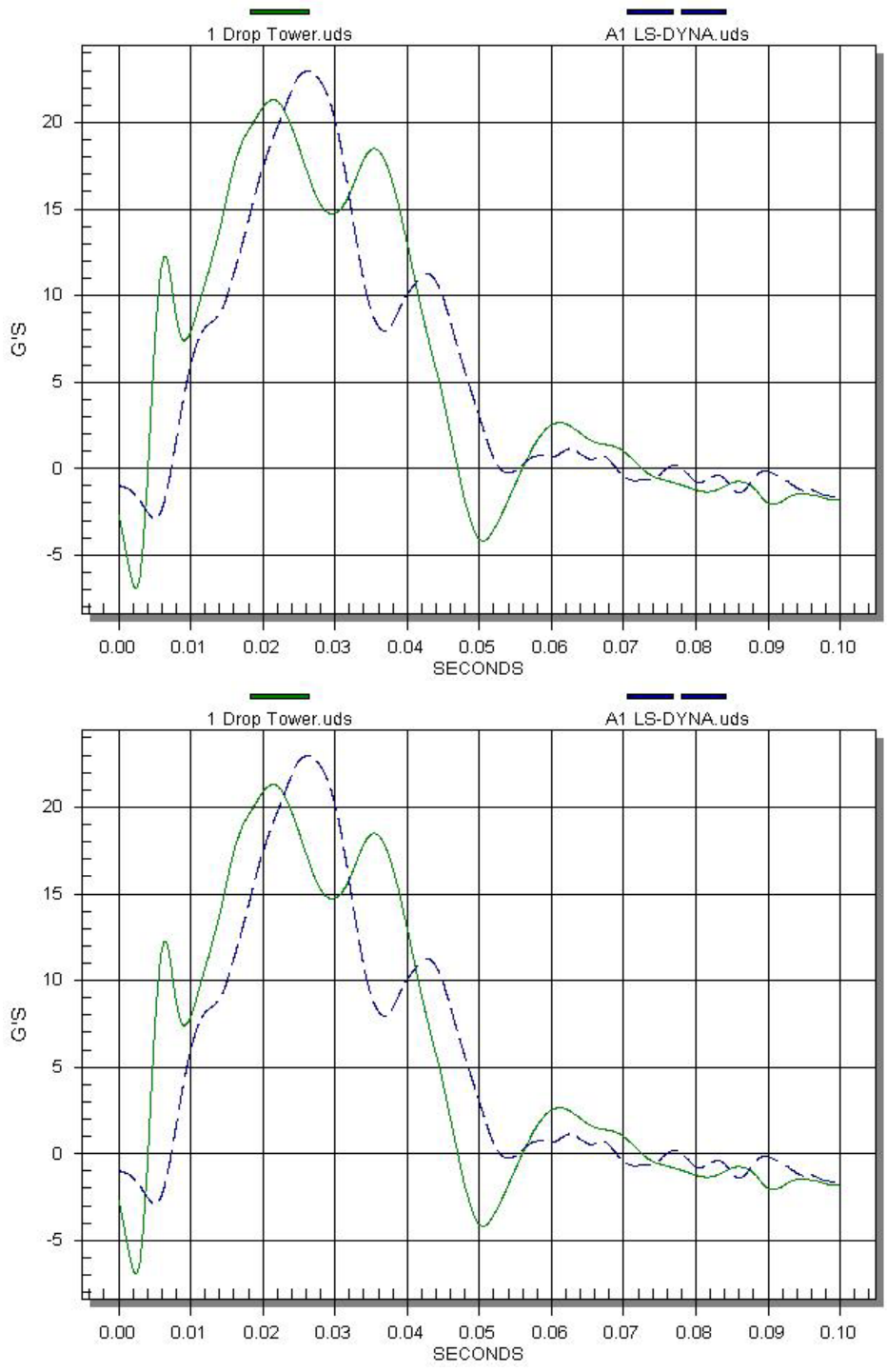


FIGURE 7-1. PELVIS ACCELERATION, 1-meter DROP, FILTERED USING A CLASS 60 FILTER

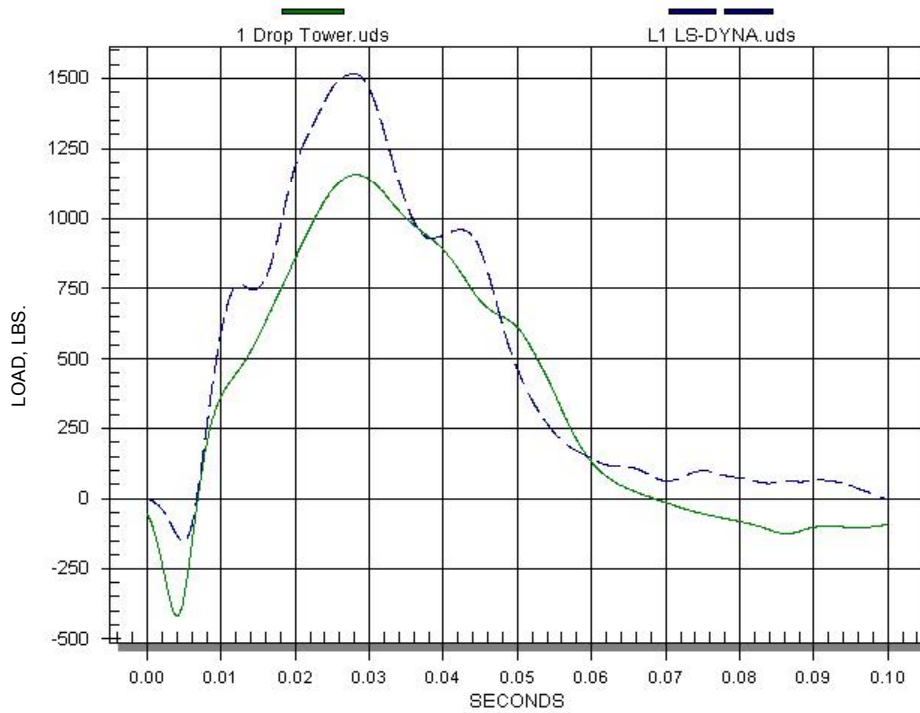


FIGURE 7-2. LUMBAR LOAD, 1-meter DROP, FILTERED USING A CLASS 60 FILTER

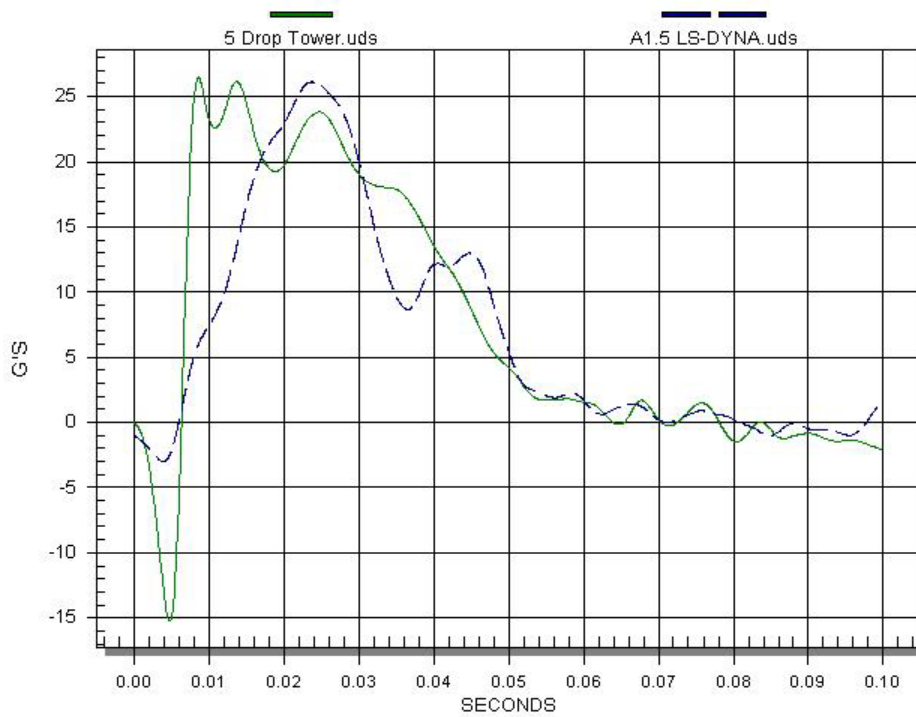


FIGURE 7-3. PELVIS ACCELERATION, 1.5-meter DROP, FILTERED USING A CLASS 60 FILTER

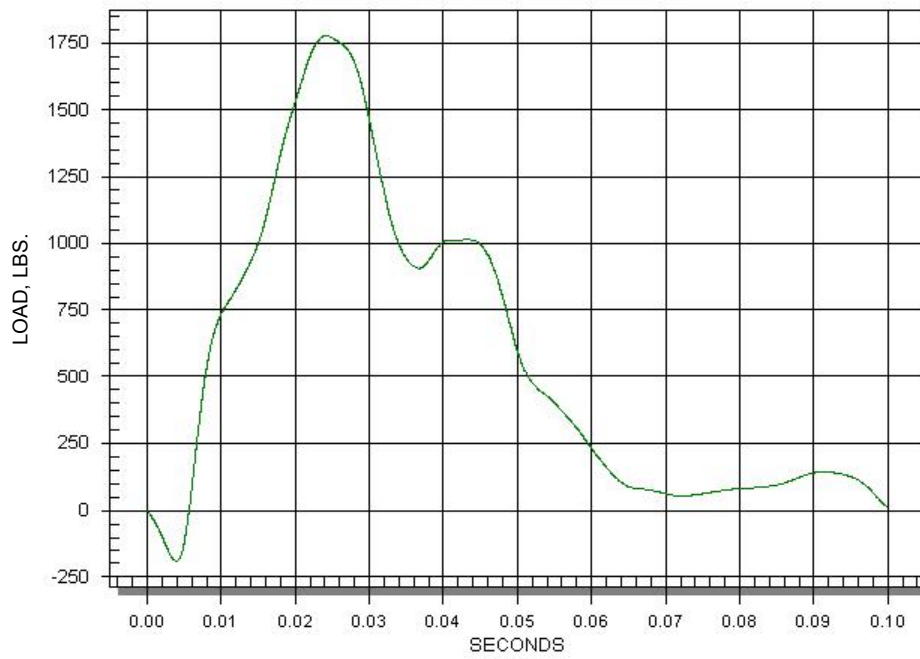


FIGURE 7-4. LUMBAR LOAD, 1.5-meter DROP, FILTERED USING A CLASS 60 FILTER

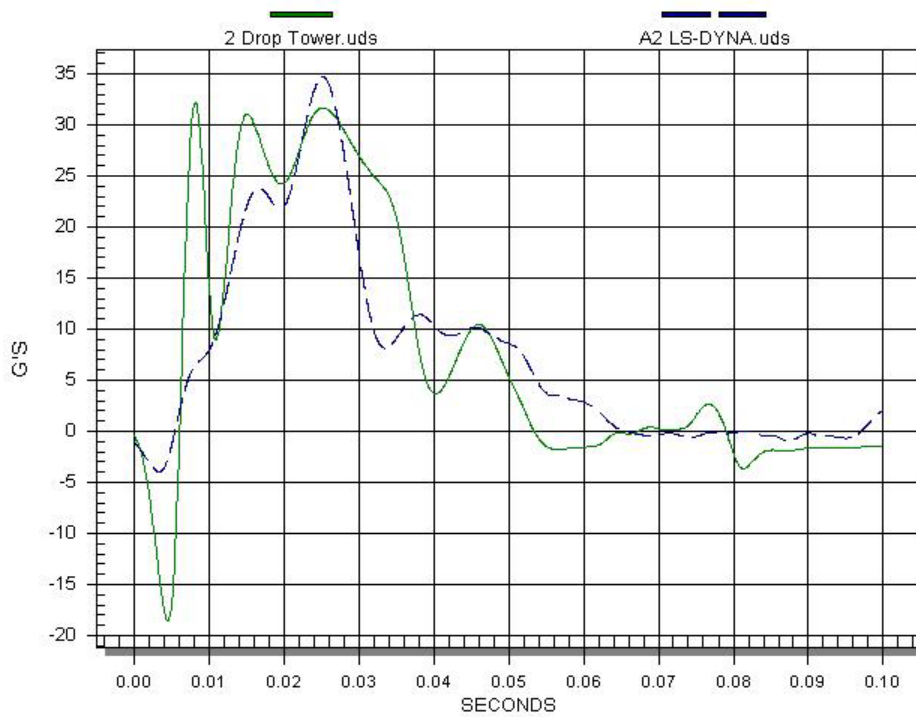


FIGURE 7-5. PELVIS ACCELERATION, 2-meter DROP, FILTERED USING A CLASS 60 FILTER

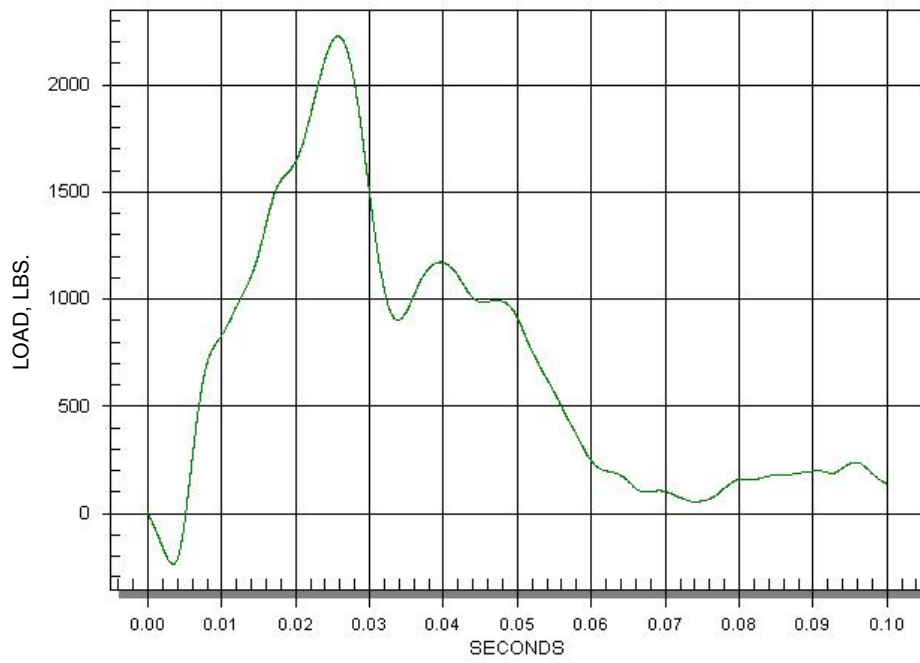


FIGURE 7-6. LUMBAR LOAD, 2-meter DROP, FILTERED USING A CLASS 60 FILTER

8. SUMMARY.

This research program has successfully developed a nonlinear finite element model of a commuter category aircraft seat subjected to severe, but survivable, crashes. The research program used a Beechcraft 1900C passenger seat as a reference commuter category aircraft seat for model development and testing. The finite element model has been used to simulate impact tests of the reference seat with an instrumented dummy at increasingly severe impact velocities. The research effort has also completed a parallel experimental program, conducted to validate the model, in which instrumented crash dummies were drop tested in the reference seat at the same impact velocities as the simulation. The resulting model will serve as a computational tool for the future evaluation and development of energy absorbing seats for commuter category aircraft.

9. REFERENCES.

1. McGuire, R. and Vu, T., "Vertical Drop Test of a Beechcraft 1900C Airliner," FAA report DOT/FAA/AR-96/119, May 1998.
2. Abramowitz, A., Ingraham, P.A., and McGuire, R., "Vertical Drop Test of a Shorts 3-30 Airplane," FAA report DOT/FAA/AR-99/87, November 1999.
3. McGuire, R.J., Nissley, W.J., and Newcomb, J.E., "Vertical Drop Test of a Metro III Aircraft," FAA report DOT/FAA/CT-93/1, June 1993.
4. Abramowitz, A., Smith, T.G., Vu, T., Zvanya, J.R., "Vertical Drop Test of a Narrow-Body Transport Fuselage Section With Overhead Stowage Bins," SAE Paper 2002-01-2995, November 2002.

APPENDIX A—TEST REPORT FOR 1-meter DROP TOWER TEST OF A BEECHCRAFT 1900C PASSENGER SEAT

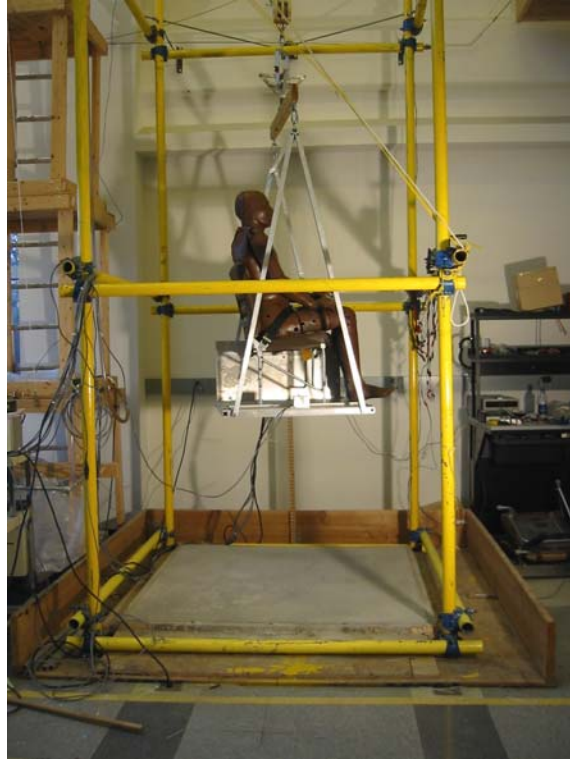


FIGURE A-1. SEAT/DUMMY ASSEMBLY AT DROP HEIGHT JUST PRIOR TO DROP



FIGURE A-2. SIDE VIEW—PRIOR TO PLATFORM ELEVATION



FIGURE A-3. SIDE VIEW—POSTTEST



FIGURE A-4. FRONT VIEW—PRETEST



FIGURE A-5. REAR VIEW—PRETEST



FIGURE A-6. FRONT VIEW—POSTTEST



FIGURE A-7. REAR VIEW—POSTTEST



FIGURE A-8. FRONT VIEW OF SIDEWALL ATTACHMENT DEFORMATION



FIGURE A-9. REAR VIEW OF SIDEWALL ATTACHMENT DEFORMATION

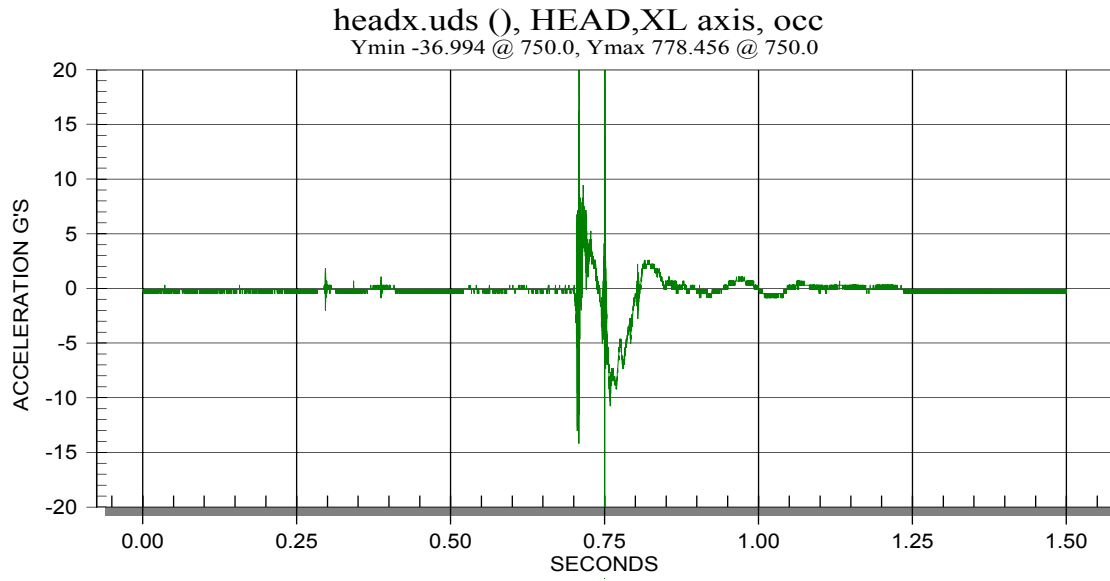


FIGURE A-10. HEAD X AXIS ACCELERATION (G's)—1000-Hz FILTER

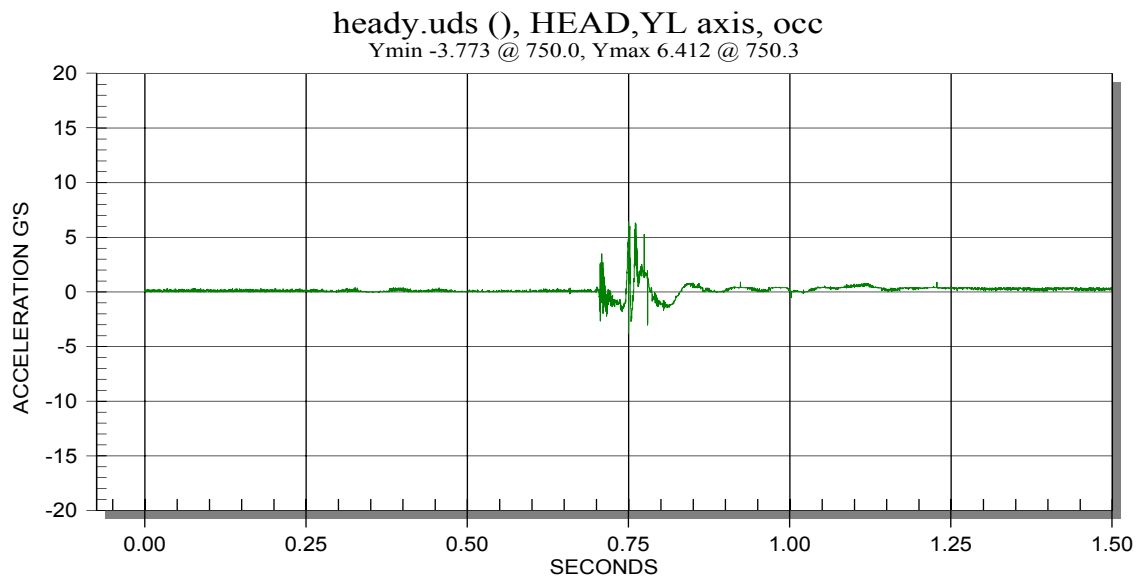


FIGURE A-11. HEAD Y AXIS ACCELERATION (G's)—1000-Hz FILTER

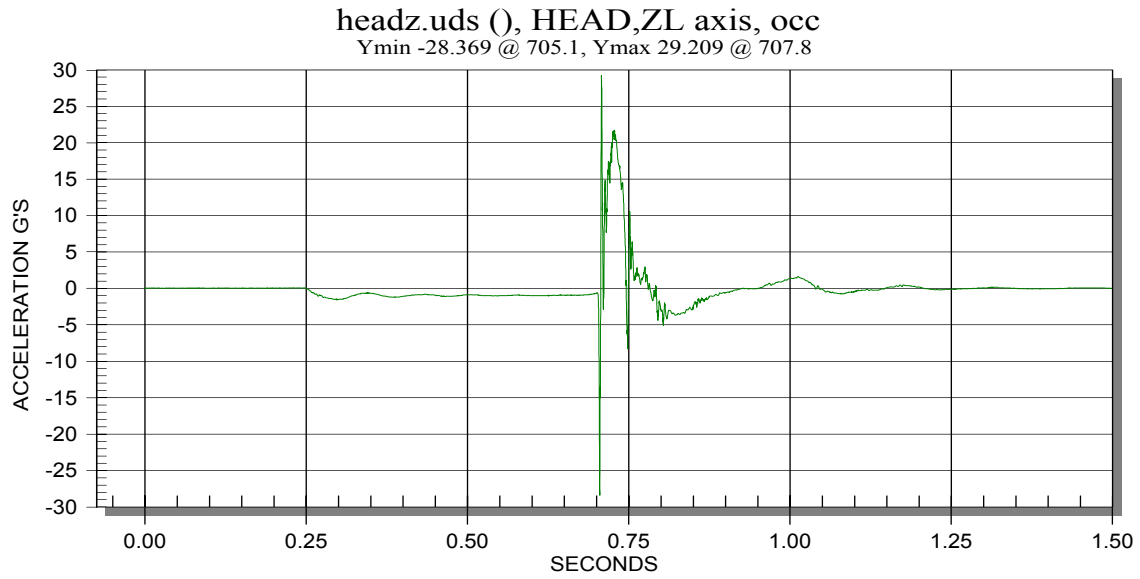


FIGURE A-12. HEAD Z AXIS ACCELERATION (G's)—1000-Hz FILTER

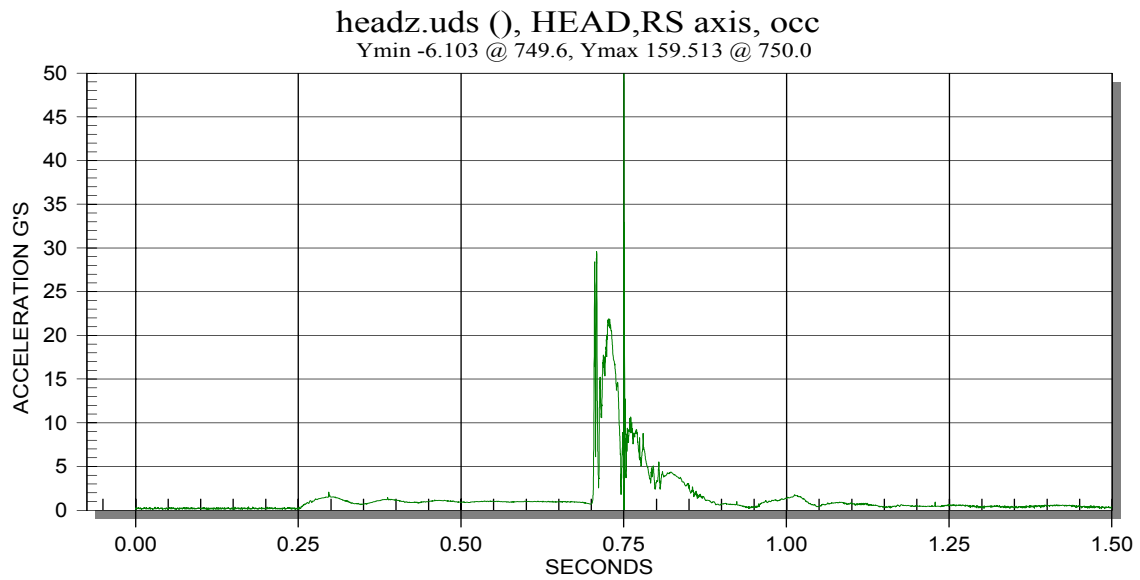


FIGURE A-13. HEAD RESULTANT ACCELERATION (G's)—1000-Hz FILTER

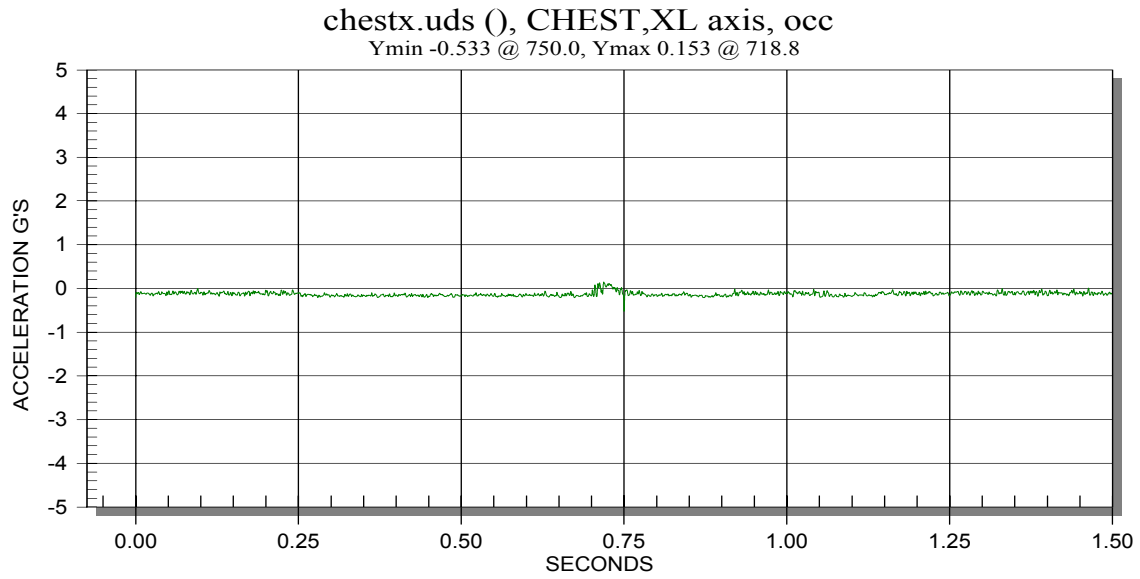


FIGURE A-14. CHEST X AXIS ACCELERATION (G's)—180-Hz FILTER

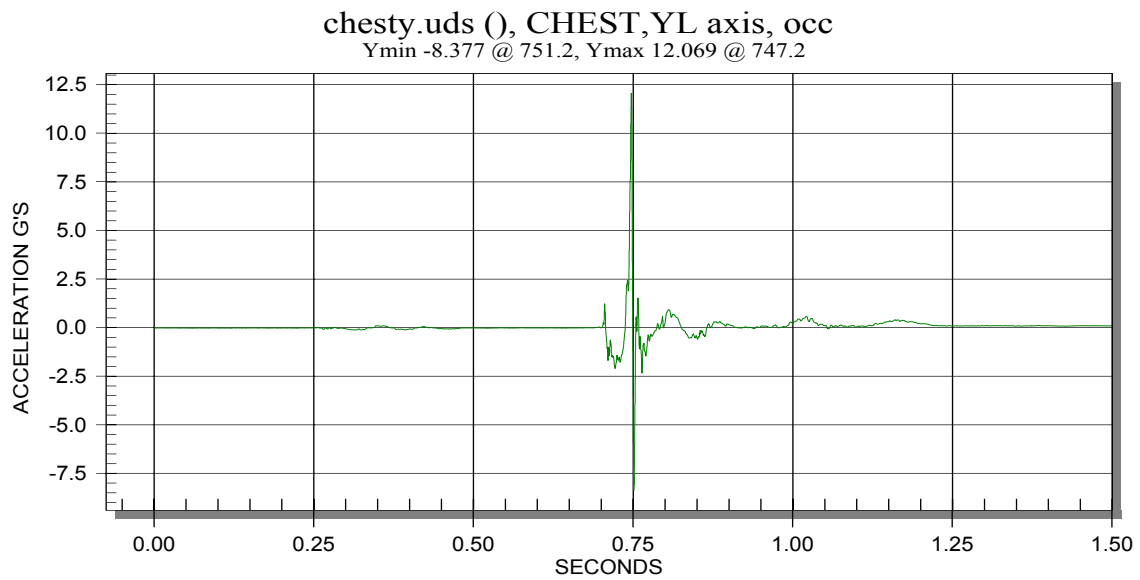


FIGURE A-15. CHEST Y AXIS ACCELERATION (G's)—180-Hz FILTER

chestz.uds (), CHEST,ZL axis, occ
Ymin -21.380 @ 704.1, Ymax 23.862 @ 728.3

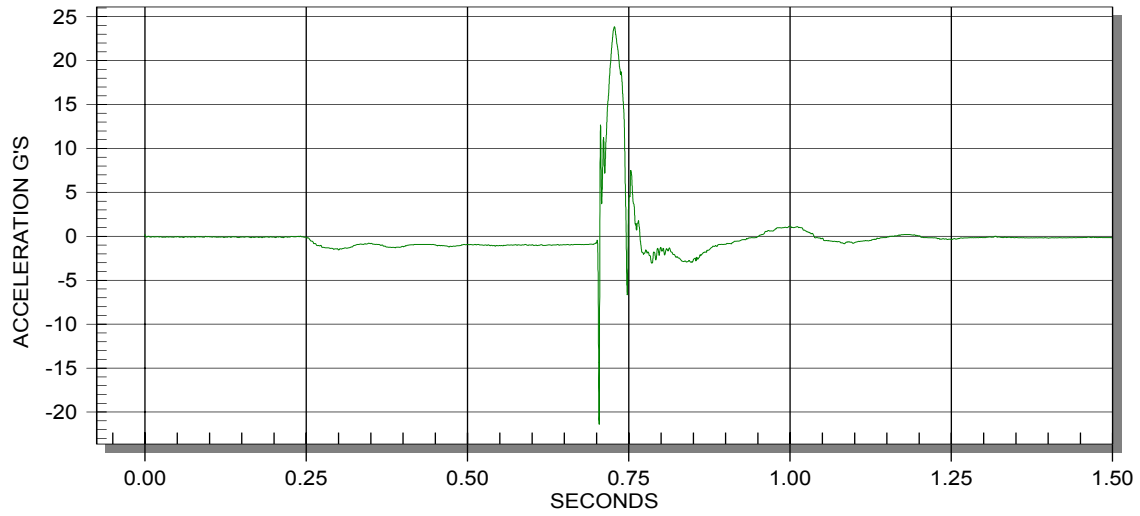


FIGURE A-16. CHEST Z AXIS ACCELERATION (G's)—180-Hz FILTER

chestz.uds (), CHEST,RS axis, occ
Ymin 0.255 @ 181.1, Ymax 24.629 @ 747.1

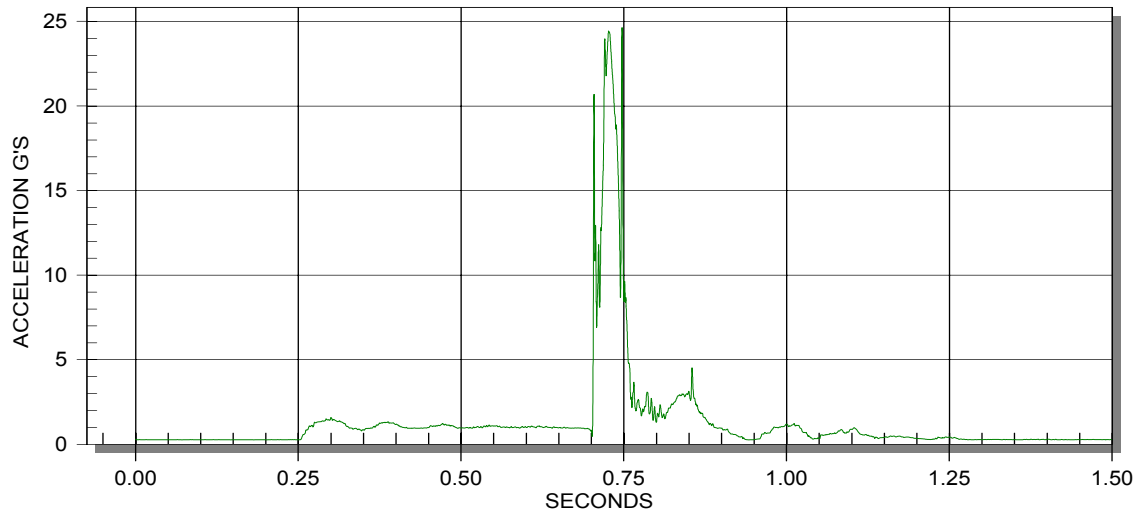


FIGURE A-17. CHEST RESULTANT ACCELERATION (G's)—180-Hz FILTER

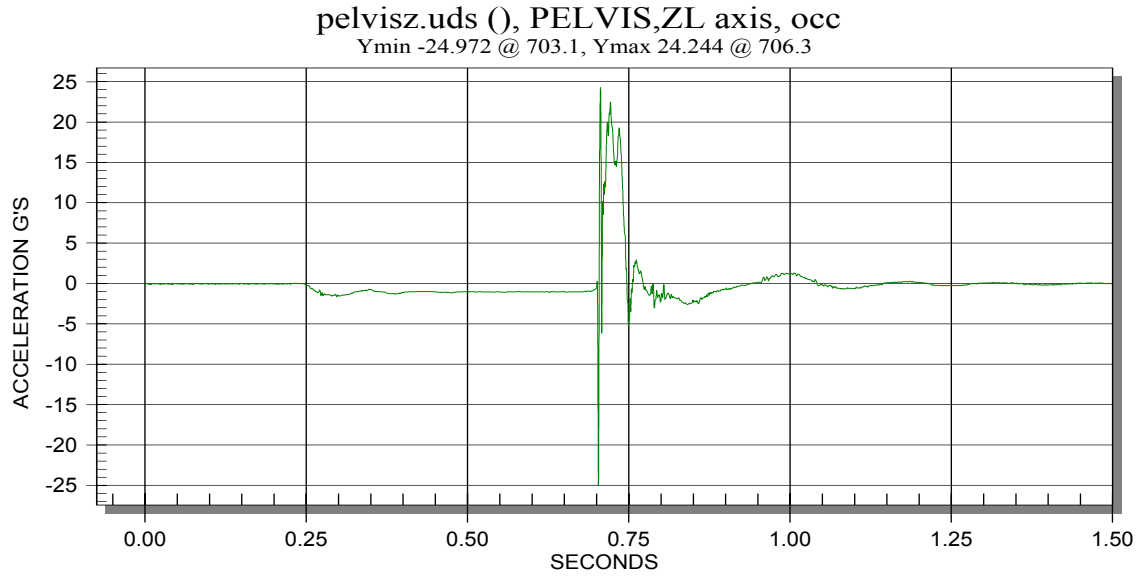


FIGURE A-18. PELVIS Z AXIS ACCELERATION (G's)—180-Hz FILTER

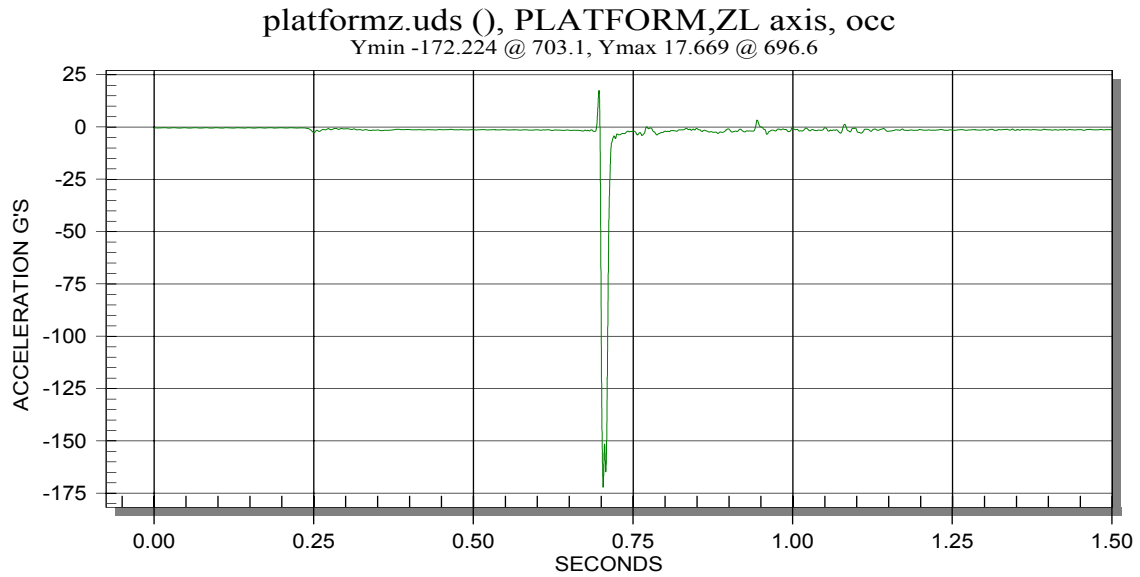


FIGURE A-19. PLATFORM Z AXIS ACCELERATION (G's)—60-Hz FILTER

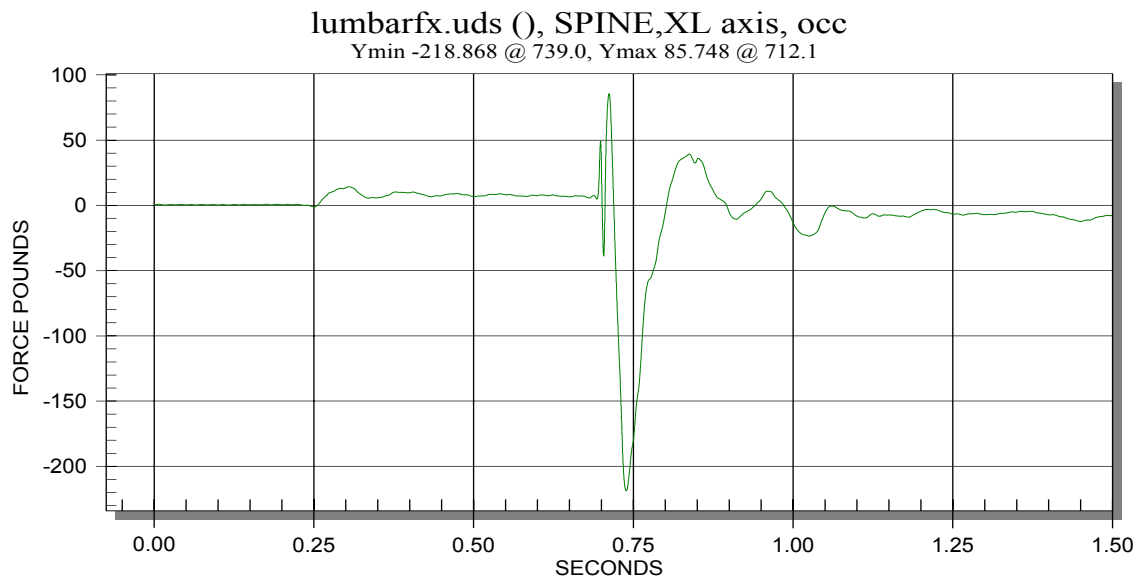


FIGURE A-20. LUMBAR LOAD CELL X AXIS FORCE (lb)—60-Hz FILTER

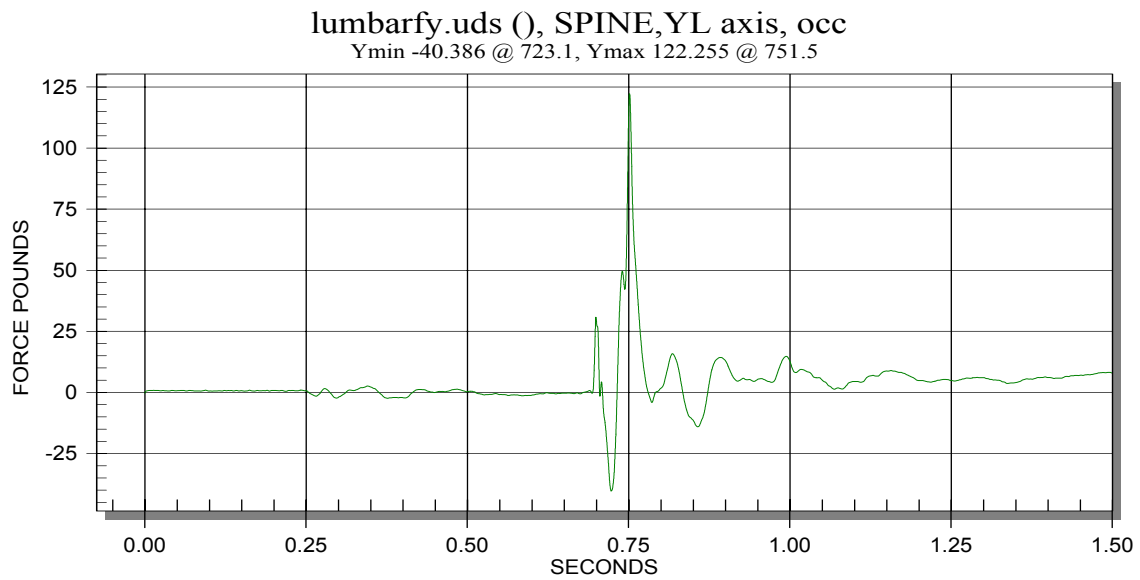


FIGURE A-21. LUMBAR LOAD CELL Y AXIS FORCE (lb)—60-Hz FILTER

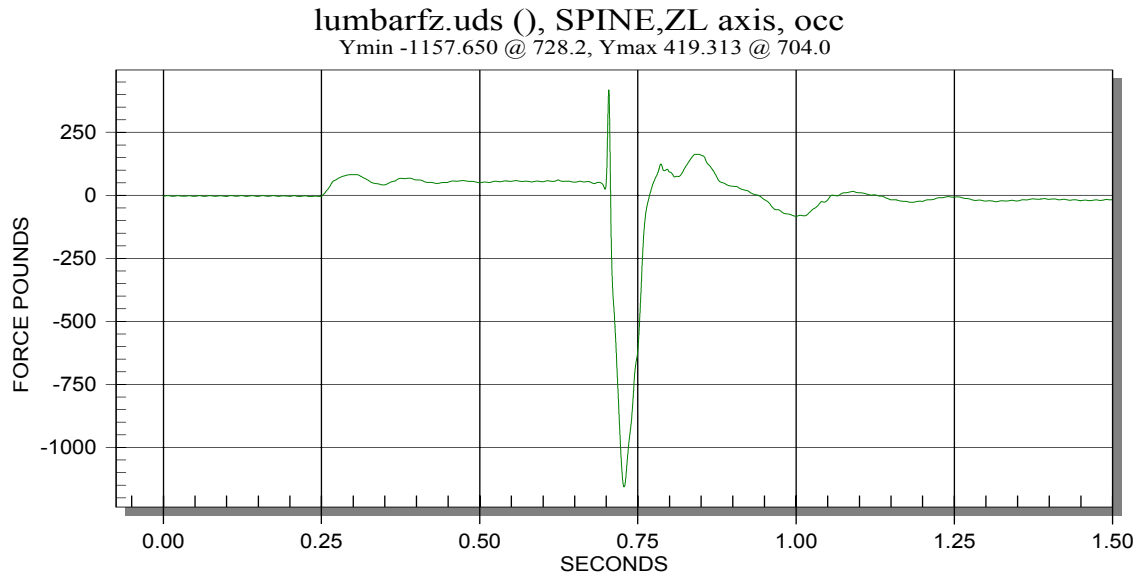


FIGURE A-22. LUMBAR LOAD CELL Z AXIS FORCE (lb)—60-Hz FILTER

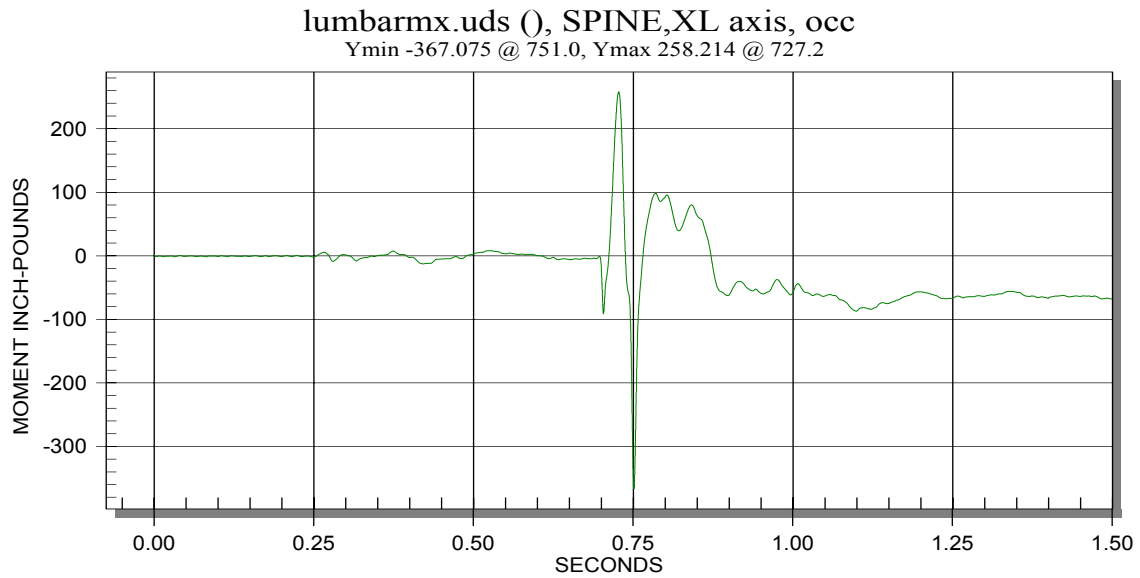


FIGURE A-23. LUMBAR LOAD CELL MOMENT X AXIS (lbs-in)—60-Hz FILTER

lumbarmy.uds (), SPINE, YL axis, occ
Ymin -517.180 @ 740.4, Ymax 331.497 @ 713.9

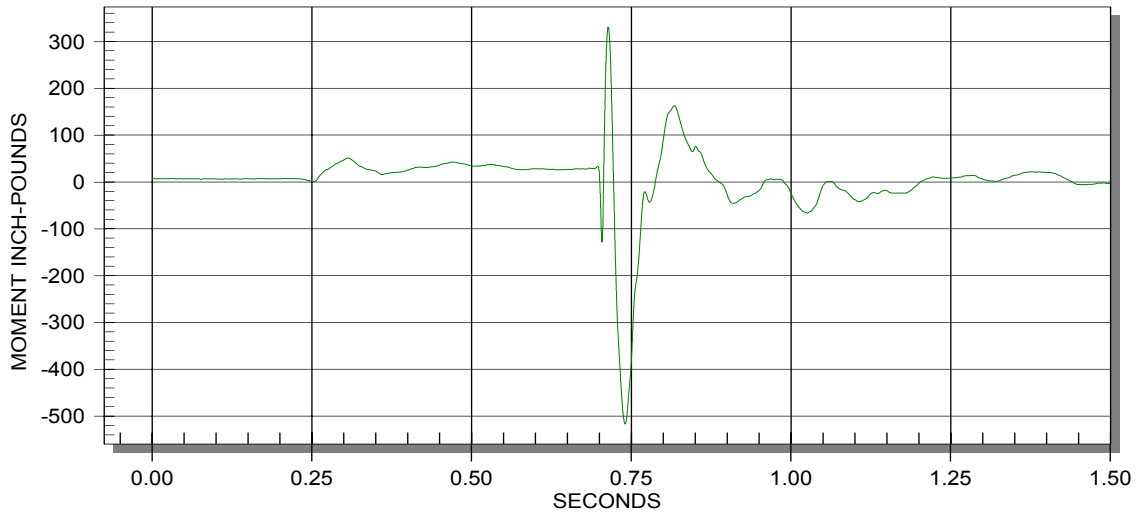


FIGURE A-24. LUMBAR LOAD CELL MOMENT Y AXIS (lbs-in)—60-Hz FILTER

lumbarz.uds (), SPINE, ZL axis, occ
Ymin -11.876 @ 742.6, Ymax 58.905 @ 1089.7

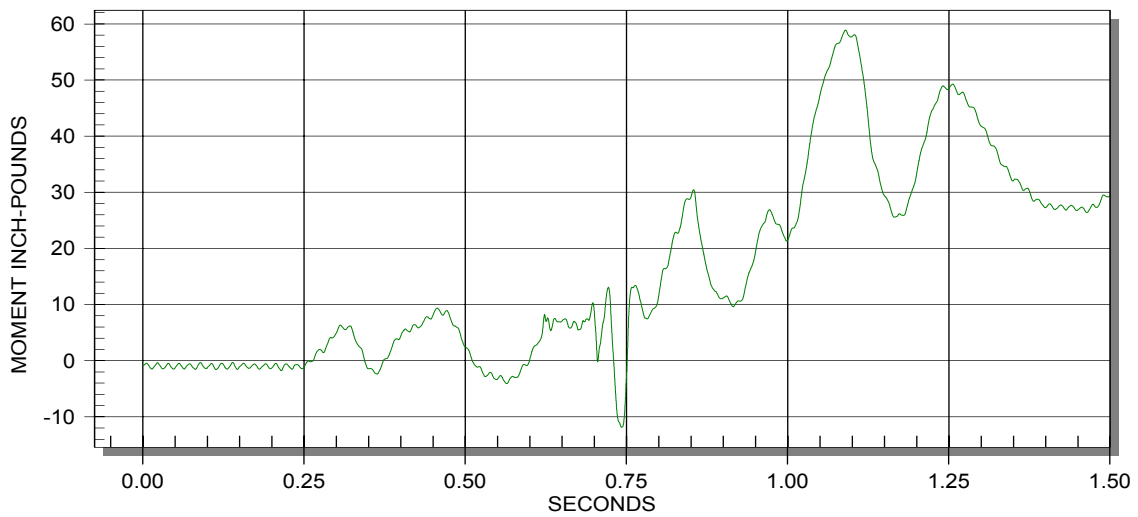


FIGURE A-25. LUMBAR LOAD CELL MOMENT Z AXIS (lbs-in)—60-Hz FILTER

APPENDIX B—TEST REPORT FOR 1.5-meter DROP TOWER TEST OF A
BEECHCRAFT 1900C PASSENGER SEAT



FIGURE B-1. SEAT/DUMMY ASSEMBLY AT DROP HEIGHT JUST PRIOR TO DROP

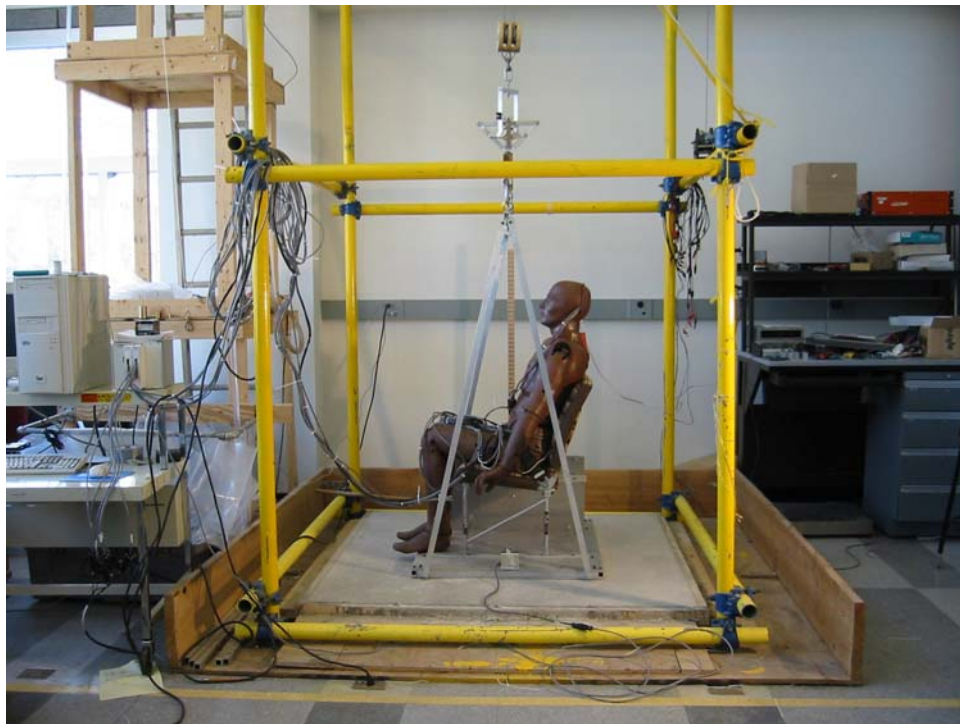


FIGURE B-2. SIDE VIEW—PRETEST



FIGURE B-3. SIDE VIEW—POSTTEST



FIGURE B-4. REAR VIEW—PRETEST



FIGURE B-5. REAR VIEW—POSTTEST



FIGURE B-6. FRONT VIEW—PRETEST



FIGURE B-7. FRONT VIEW—POSTTEST



FIGURE B-8. FAILED SEAT BACK STOP ON LEFT SIDE

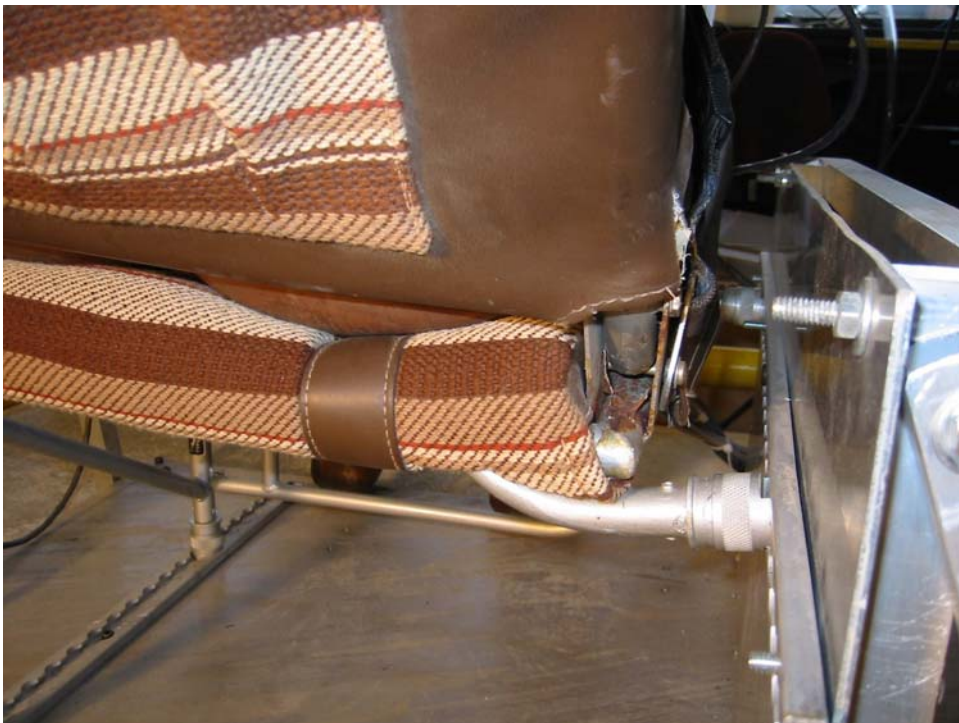


FIGURE B-9. SIDEWALL ATTACHMENT DEFORMATION AND FAILED SEAT BACK STOP ON RIGHT SIDE

HEADX.UDS (), HEAD,XL axis, occ
Ymin -51.606 @ 654.6, Ymax 60.360 @ 653.6

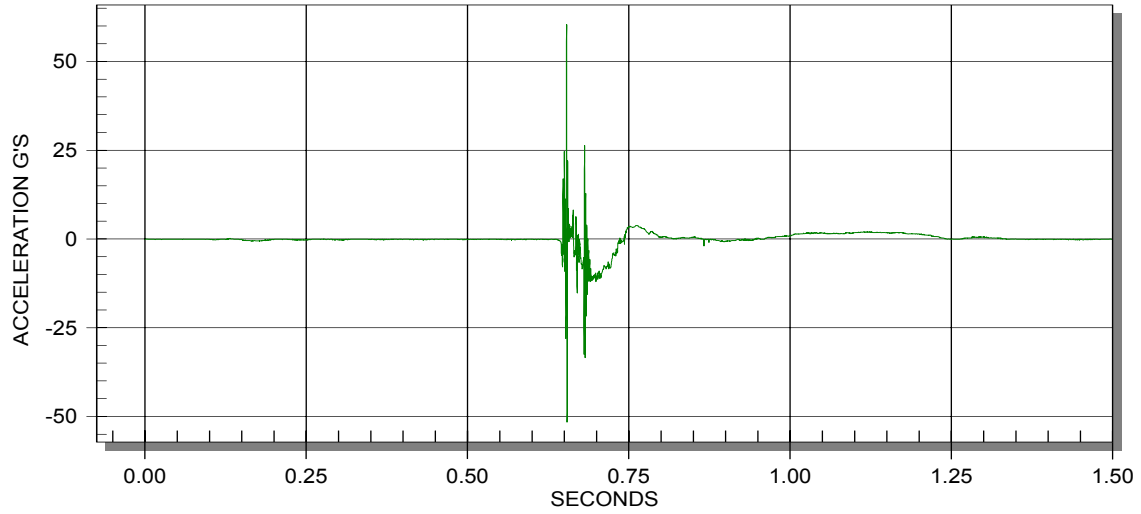


FIGURE B-10. HEAD X AXIS ACCELERATION (G's)—1000-Hz FILTER

HEADY.UDS (), HEAD,YL axis, occ
Ymin -34.297 @ 654.2, Ymax 36.077 @ 654.5

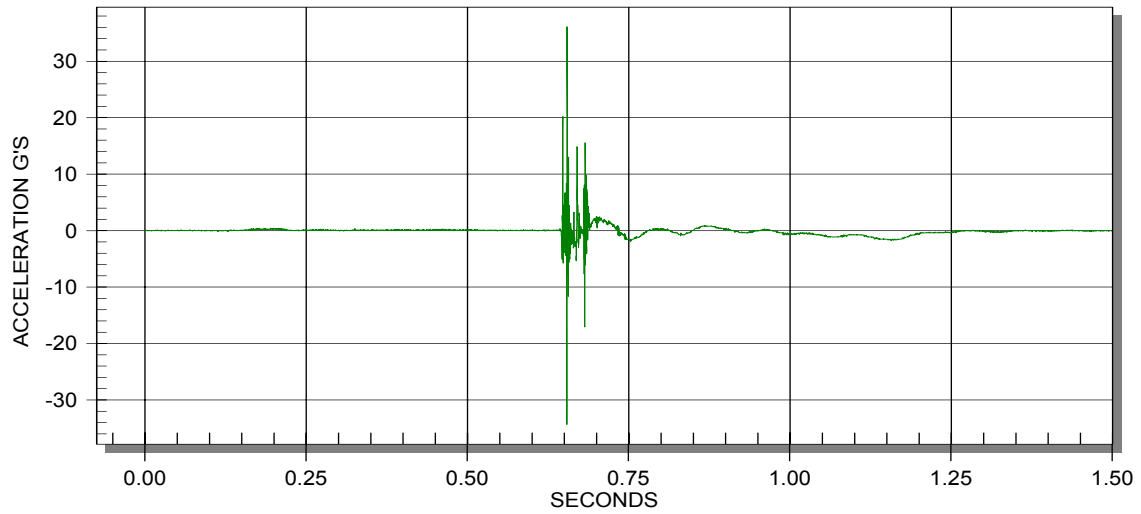


FIGURE B-11. HEAD Y AXIS ACCELERATION (G's)—1000-Hz FILTER

HEADZ.UDS (), HEAD,ZL axis, occ
Ymin -56.910 @ 648.0, Ymax 54.111 @ 650.2

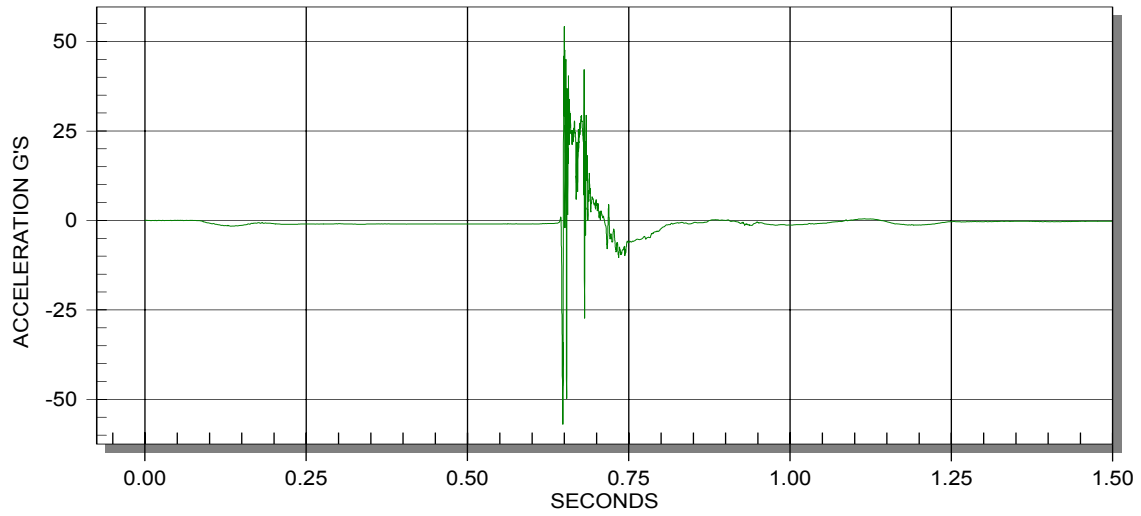


FIGURE B-12. HEAD Z AXIS ACCELERATION (G's)—1000-Hz FILTER

HEADZ.UDS (), HEAD,RS axis, occ
Ymin 0.090 @ 15.4, Ymax 91.049 @ 653.5

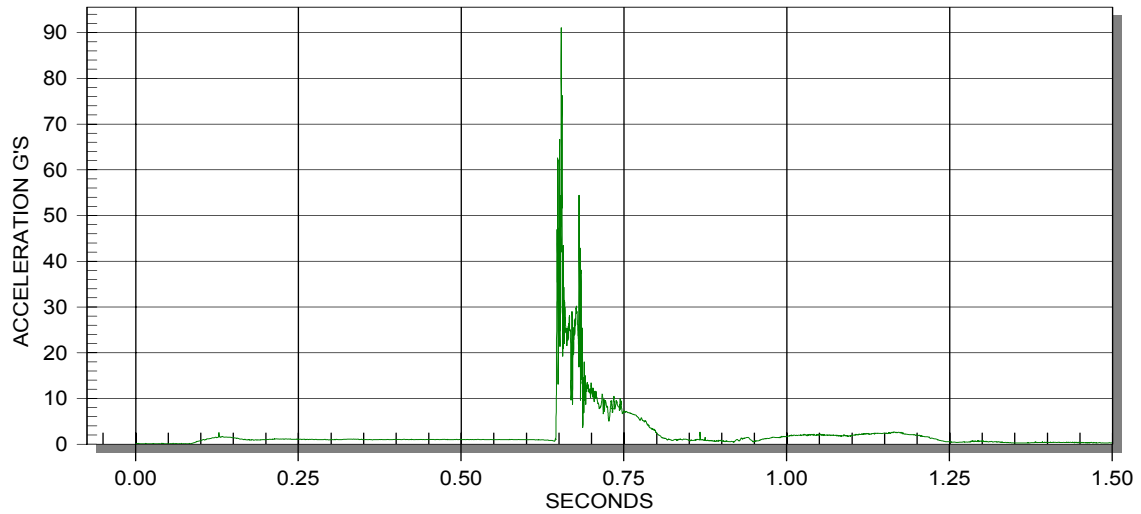


FIGURE B-13. HEAD RESULTANT ACCELERATION (G's)—1000-Hz FILTER

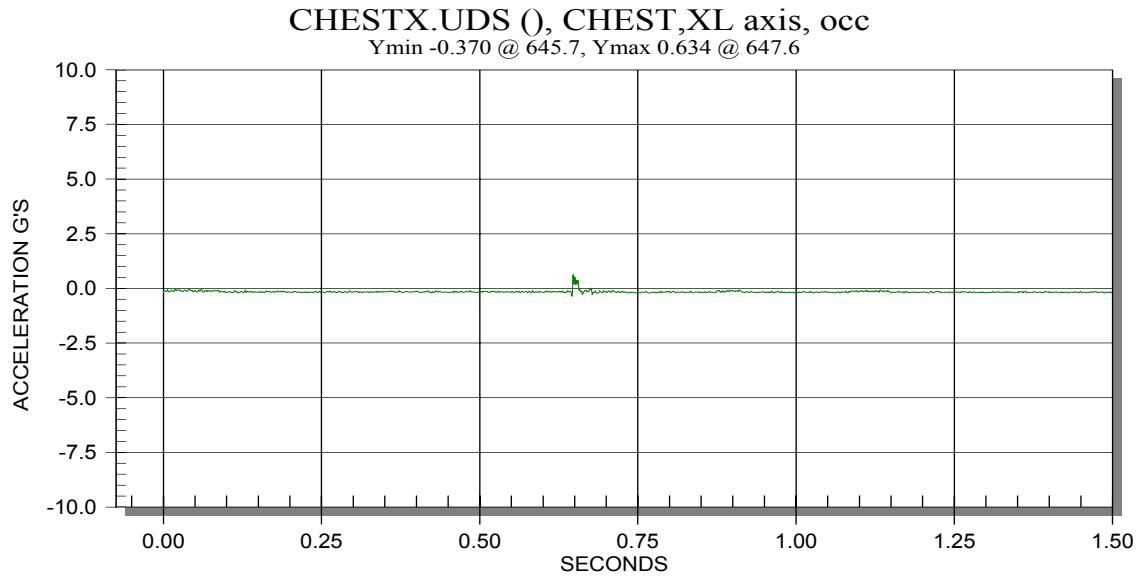


FIGURE B-14. CHEST X AXIS ACCELERATION (G's)—180-Hz FILTER

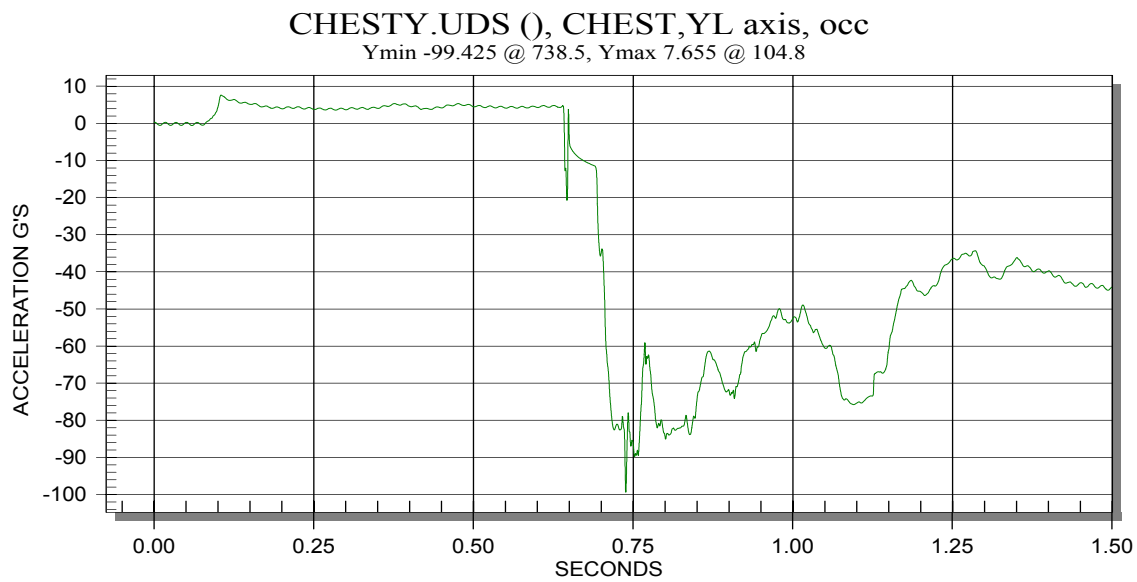


FIGURE B-15. CHEST Y AXIS ACCELERATION (G's)—180-Hz FILTER
 (QUESTIONABLE DATA)

CHESTZ.UDS (), CHEST,ZL axis, occ
Ymin -38.975 @ 646.7, Ymax 29.467 @ 673.8

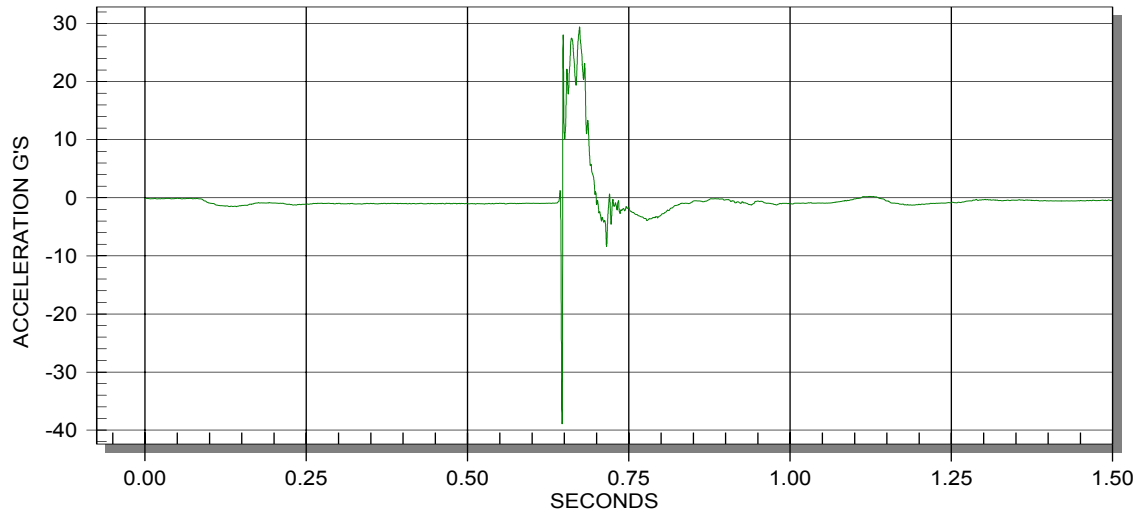


FIGURE B-16. CHEST Z AXIS ACCELERATION (G's)—180-Hz FILTER

CHESTZ.UDS (), CHEST,RS axis, occ
Ymin -0.178 @ 643.6, Ymax 40.531 @ 647.0

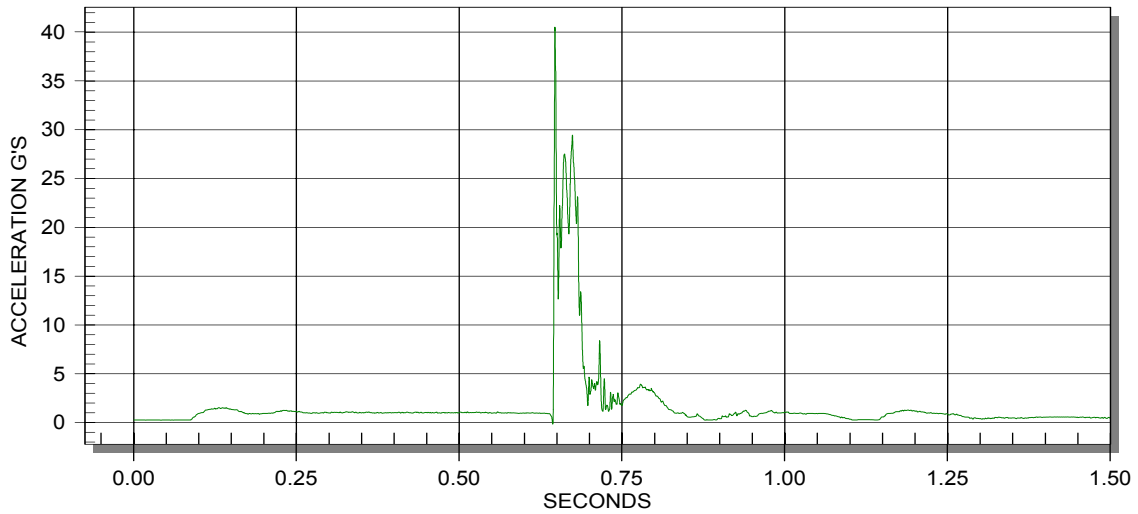


FIGURE B-17. CHEST RESULTANT ACCELERATION (G's)—(X AND Z AXIS ONLY)
180-Hz FILTER

PELVISZ.UDS (), PELVIS,ZL axis, occ
Ymin -62.187 @ 645.5, Ymax 68.252 @ 647.7

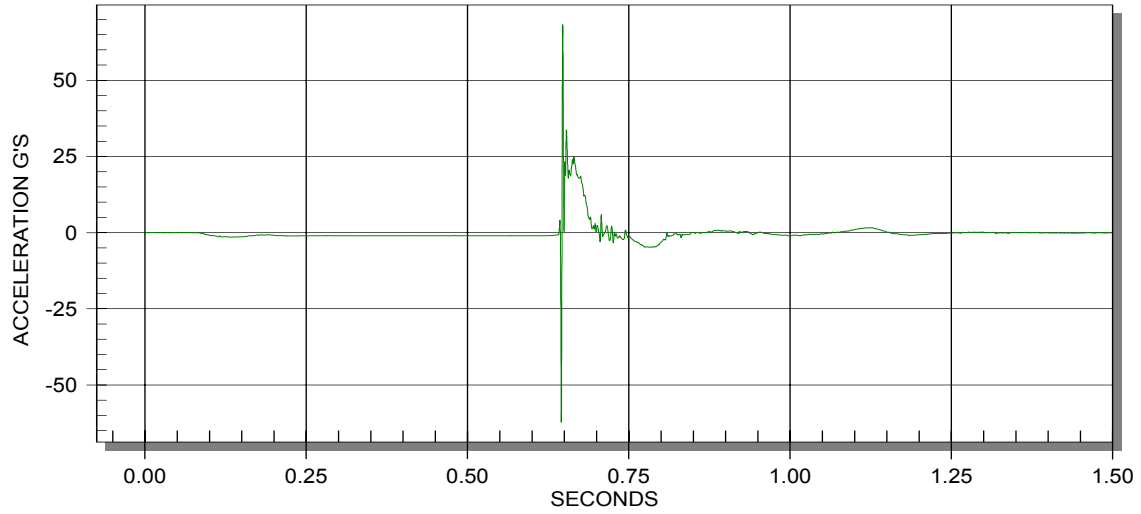


FIGURE B-18. PELVIS Z AXIS ACCELERATION (G's)—180-Hz FILTER

PLATFORMZ.UDS (), PLATFORM,ZL axis, occ
Ymin -780.133 @ 640.5, Ymax 778.225 @ 637.3

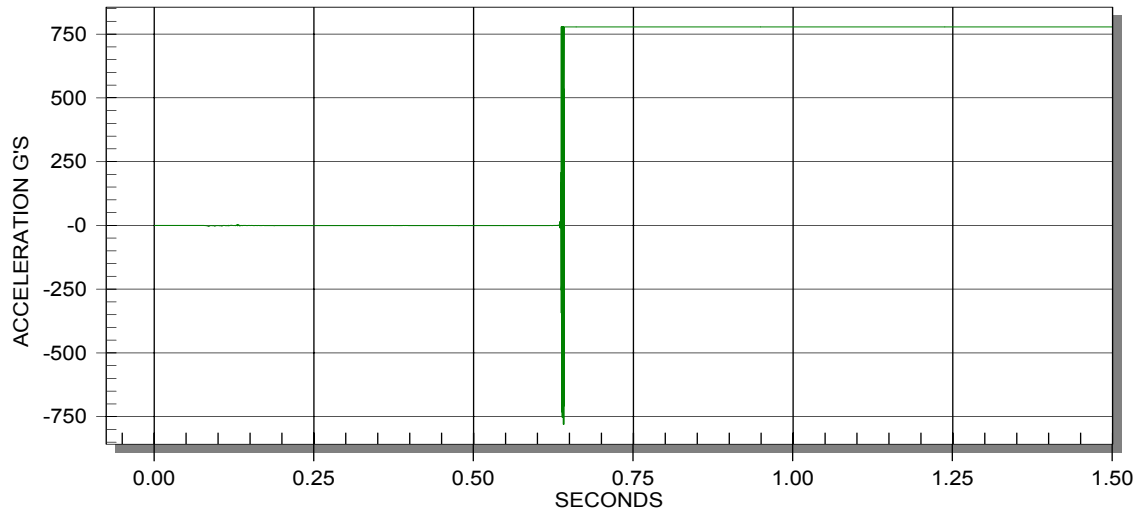


FIGURE B-19. PLATFORM Z AXIS ACCELERATION (G's)—CHANNEL FAILED

LUMBARFX.UDS (), SPINE,XL axis, occ
Ymin -12.163 @ 30.7, Ymax 3206.442 @ 640.2

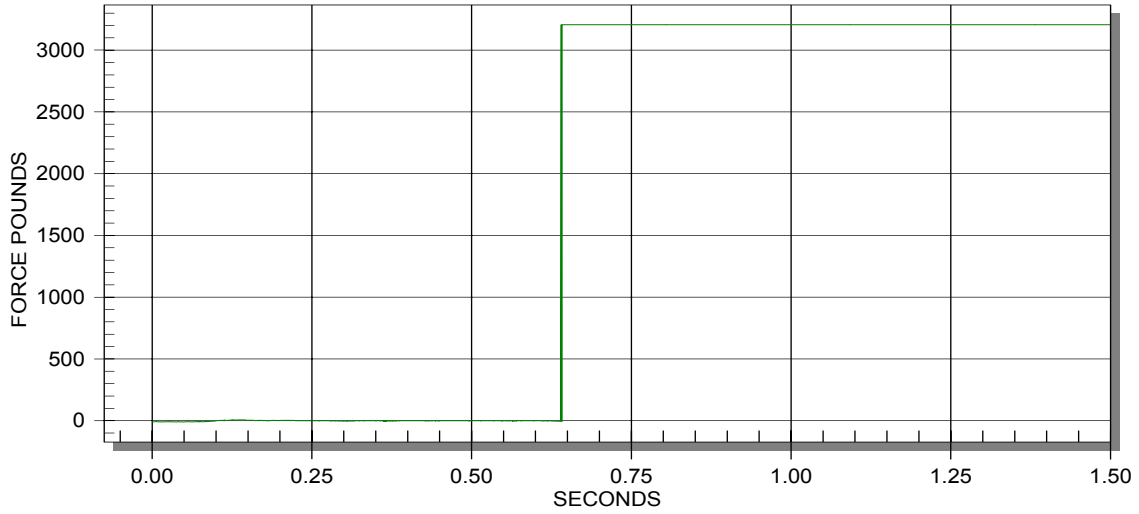


FIGURE B-20. LUMBAR LOAD CELL X AXIS FORCE (lb)—CHANNEL FAILED

LUMBARFY.UDS (), SPINE,YL axis, occ
Ymin -5.049 @ 185.9, Ymax 3209.746 @ 641.6

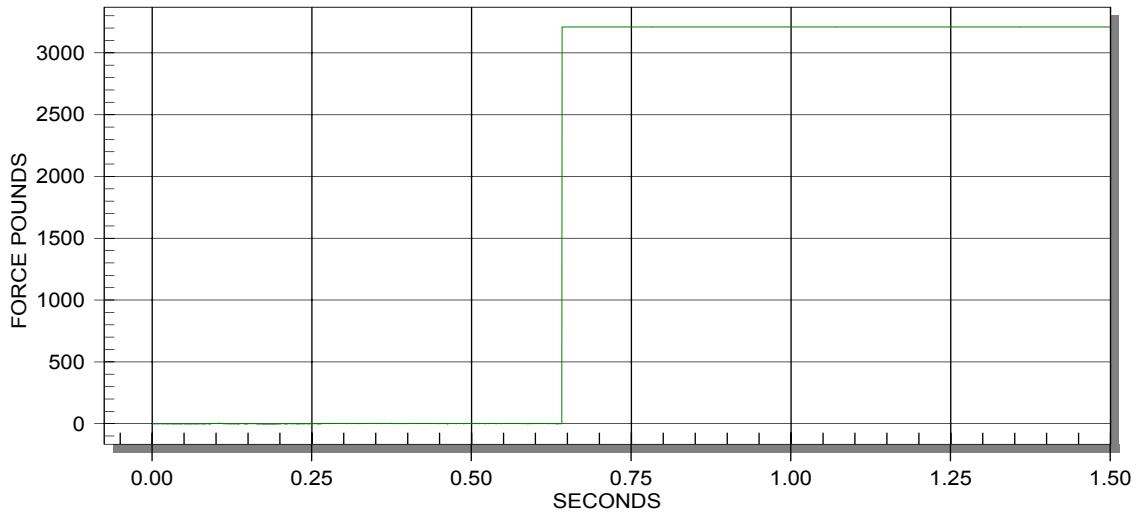


FIGURE B-21. LUMBAR LOAD CELL Y AXIS FORCE (lb)—CHANNEL FAILED

LUMBARFZ.UDS (), SPINE,ZL axis, occ
Ymin -5.211 @ 14.9, Ymax 5896.611 @ 641.7

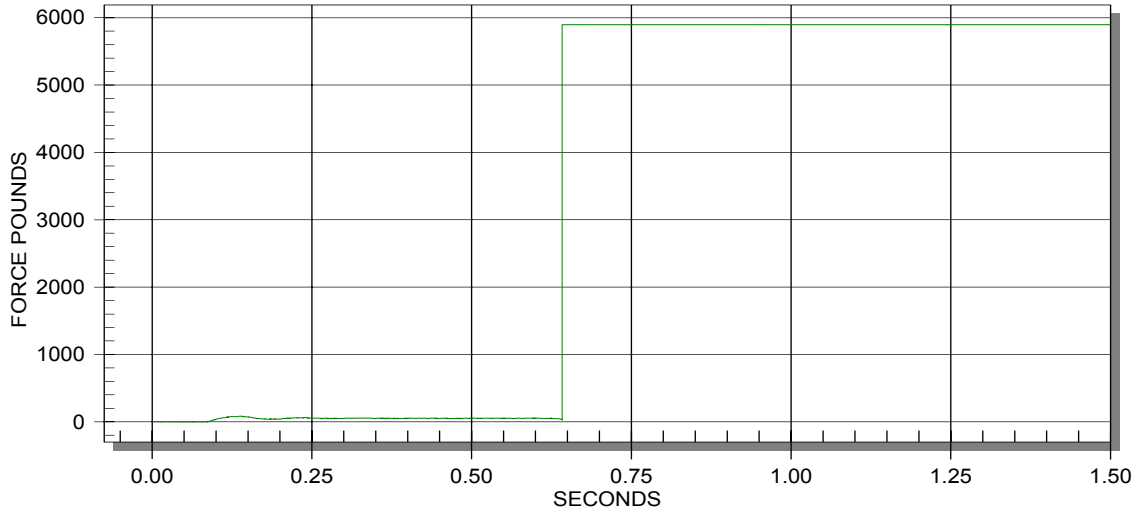


FIGURE B-22. LUMBAR LOAD CELL Z AXIS FORCE (lb)—CHANNEL FAILED

LUMBARMX.UDS (), SPINE,XL axis, occ
Ymin -254.168 @ 659.2, Ymax 202.782 @ 1121.7

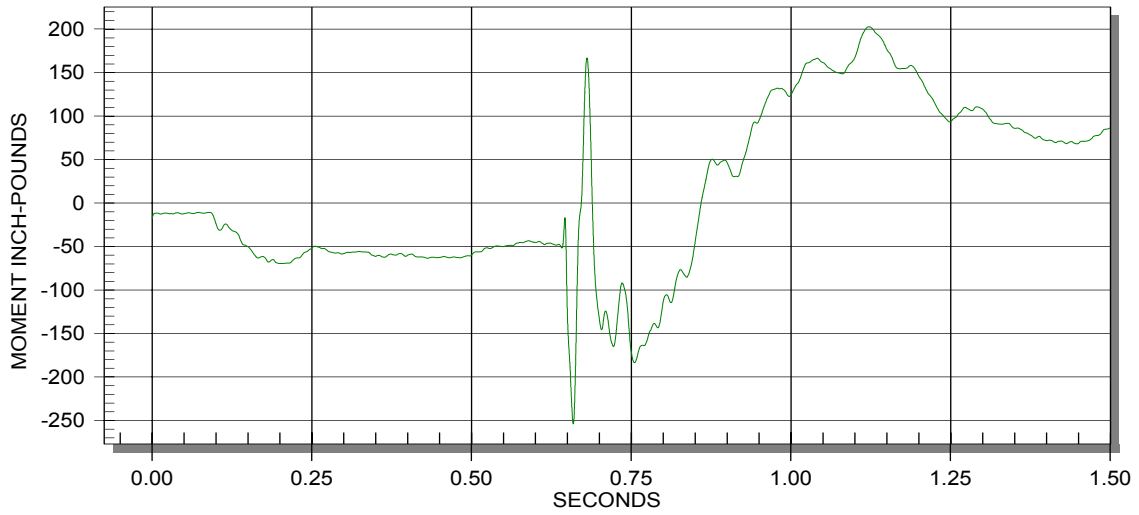


FIGURE B-23. LUMBAR LOAD CELL MOMENT X AXIS (lbs-in)—60-Hz FILTER

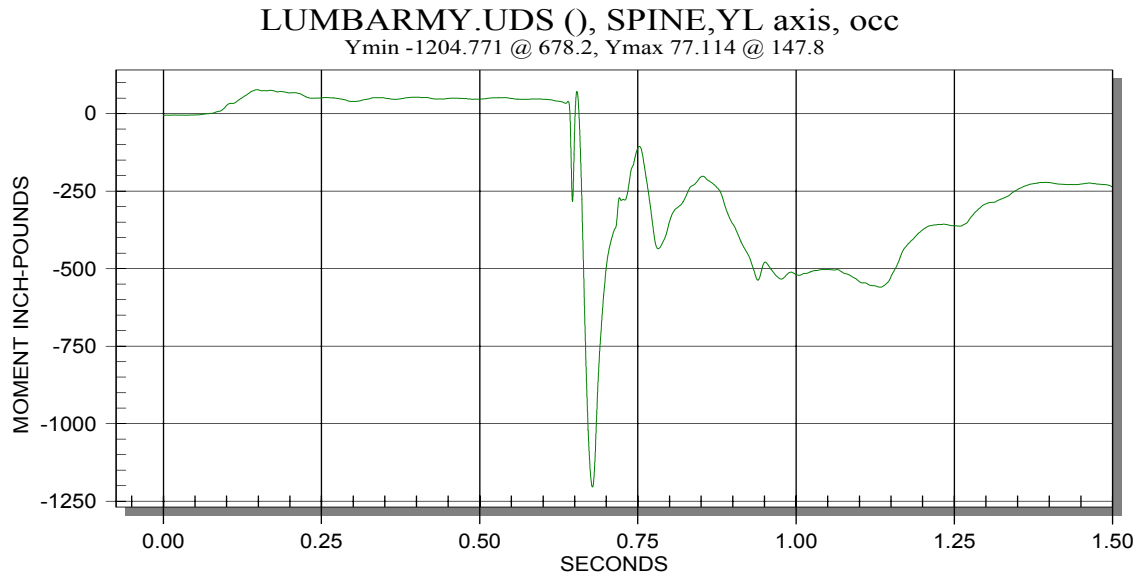


FIGURE B-24. LUMBAR LOAD CELL MOMENT Y AXIS (lbs-in)—60-Hz FILTER

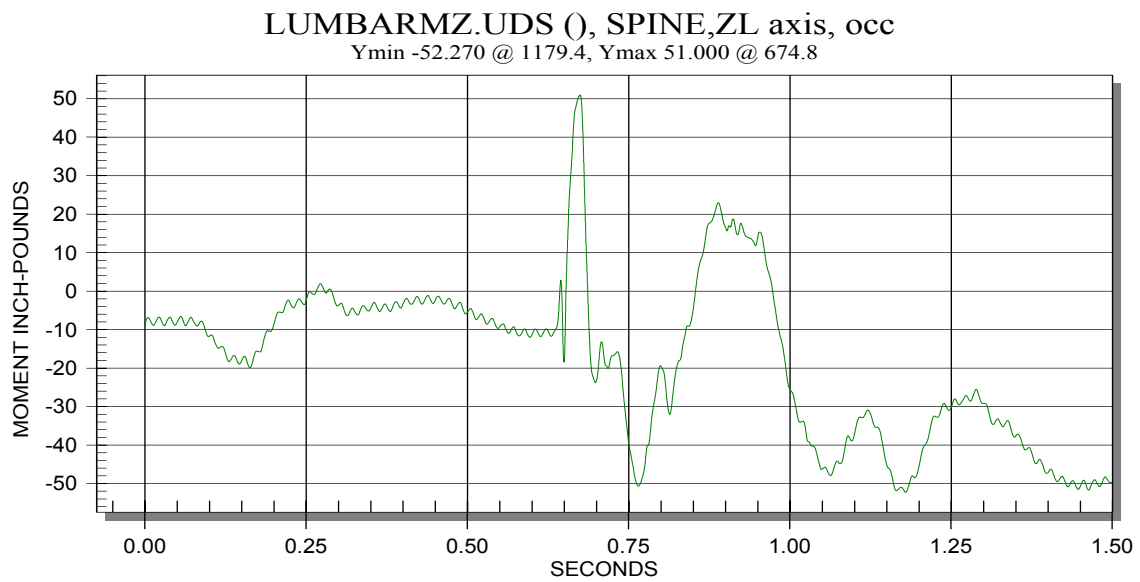


FIGURE B-25. LUMBAR LOAD CELL MOMENT Z AXIS (lbs-in)—60-Hz FILTER

APPENDIX C—TEST REPORT FOR 2-meter DROP TOWER TEST OF A
BEEHCRAFT 1900C PASSENGER SEAT



FIGURE C-1. SEAT/DUMMY ASSEMBLY AT DROP HEIGHT JUST PRIOR TO DROP



FIGURE C-2. SIDE VIEW—PRETEST

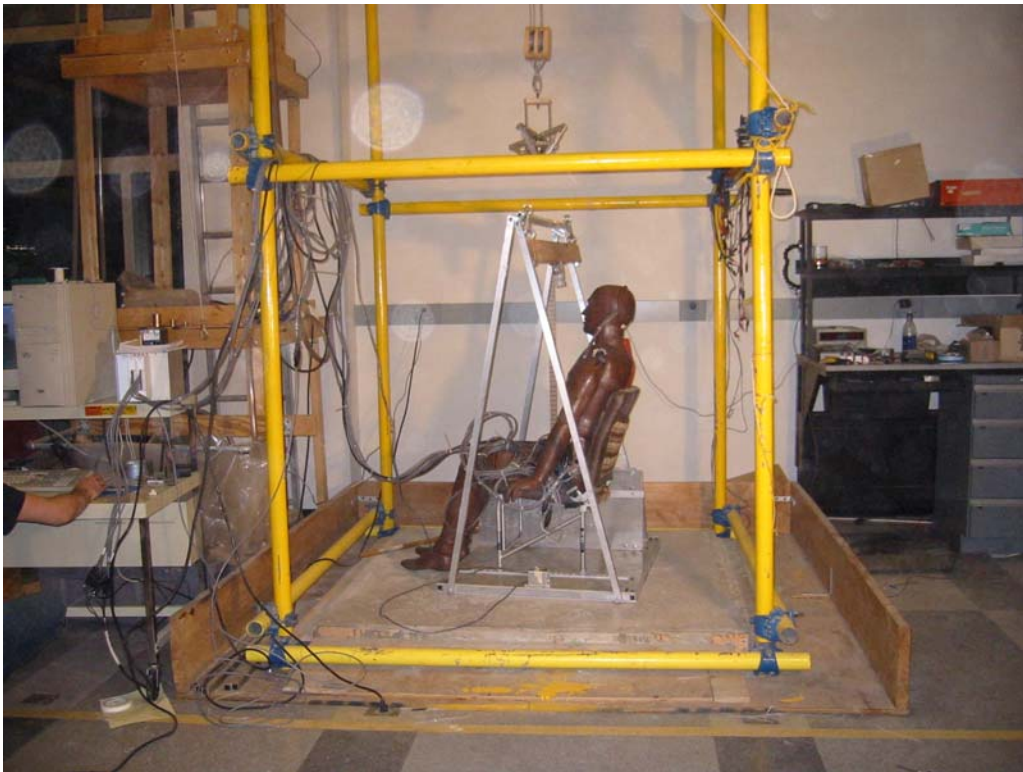


FIGURE C-3. SIDE VIEW—POSTTEST



FIGURE C-4. REAR VIEW—PRETEST



FIGURE C-5. REAR VIEW—POSTTEST



FIGURE C-6. FRONT VIEW—PRETEST



FIGURE C-7. FRONT VIEW—POSTTEST



FIGURE C-8. REAR VIEW OF SIDEWALL ATTACHMENT DEFORMATION



FIGURE C-9. FRONT VIEW OF SIDEWALL ATTACHMENT DEFORMATION



FIGURE C-10. TOP VIEW OF SIDEWALL ATTACHMENT SHOWING SLIGHT DETACHMENT OF SIDE SEAT TRACK RAIL FROM SIDEWALL

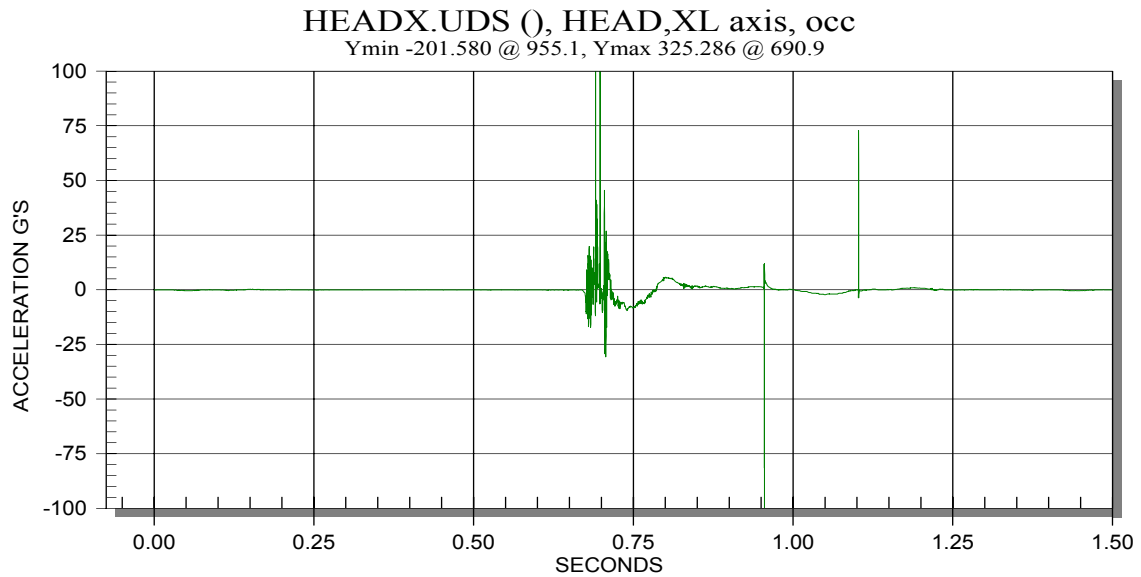


FIGURE C-11. HEAD X AXIS ACCELERATION (G's)—1000-Hz FILTER

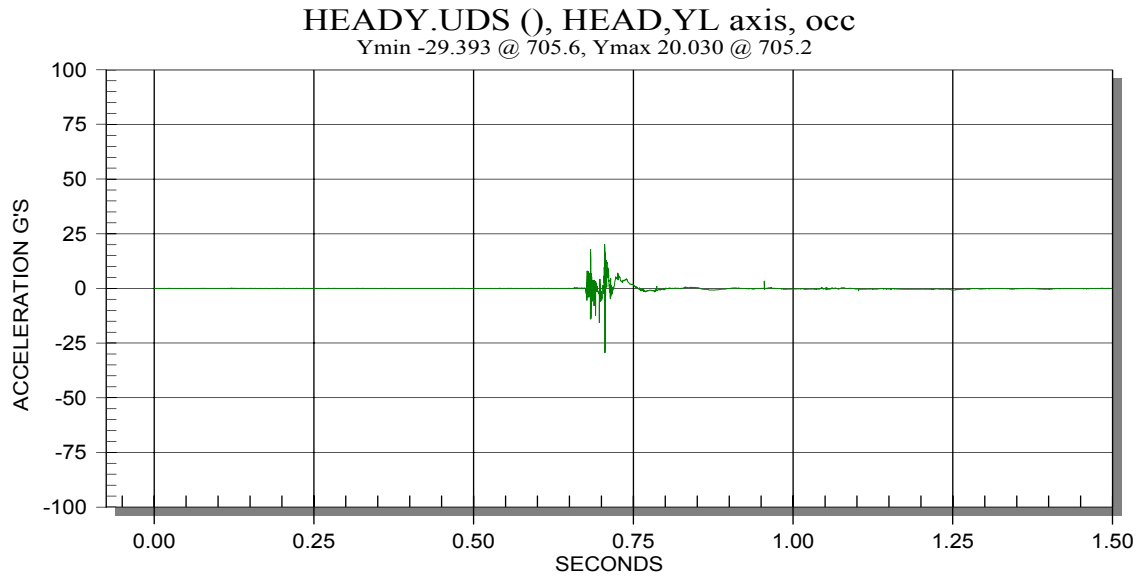


FIGURE C-12. HEAD Y AXIS ACCELERATION (G's)—1000-Hz FILTER

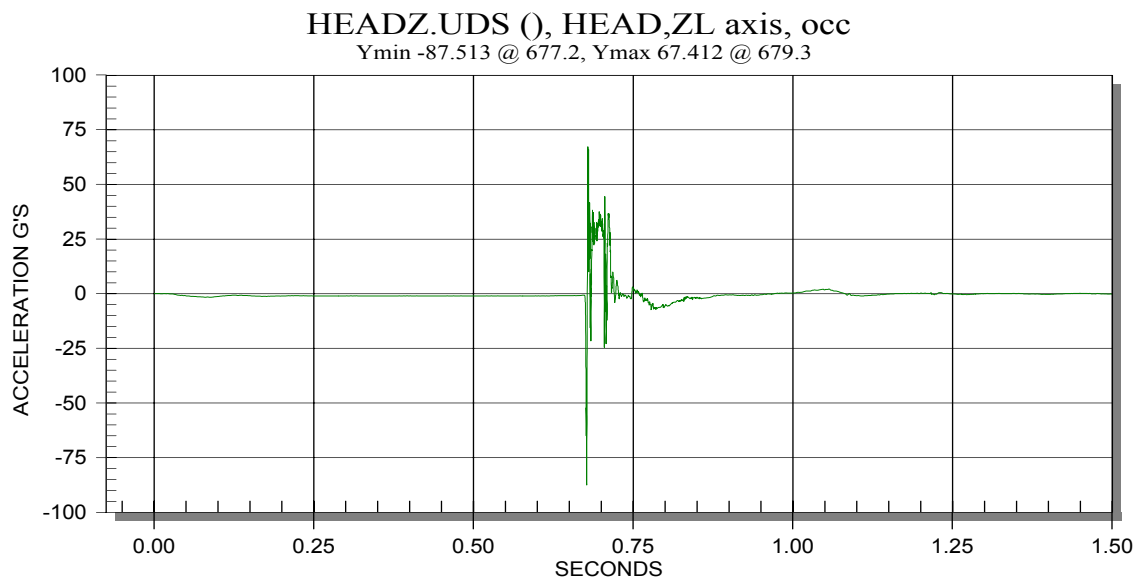


FIGURE C-13. HEAD Z AXIS ACCELERATION (G's)—1000-Hz FILTER

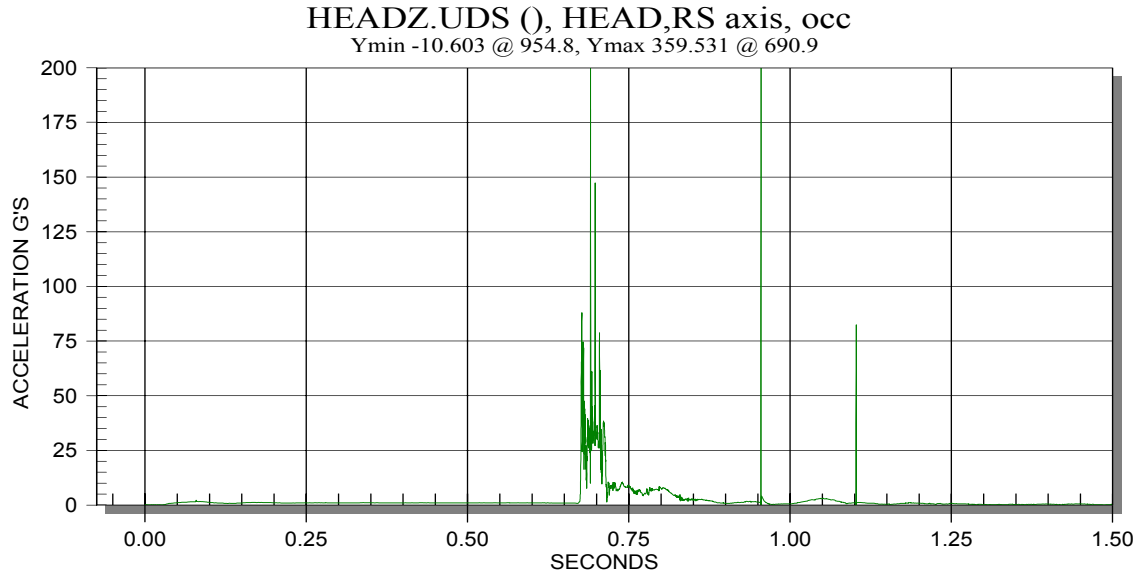


FIGURE C-14. HEAD RESULTANT ACCELERATION (G's)—1000-Hz FILTER

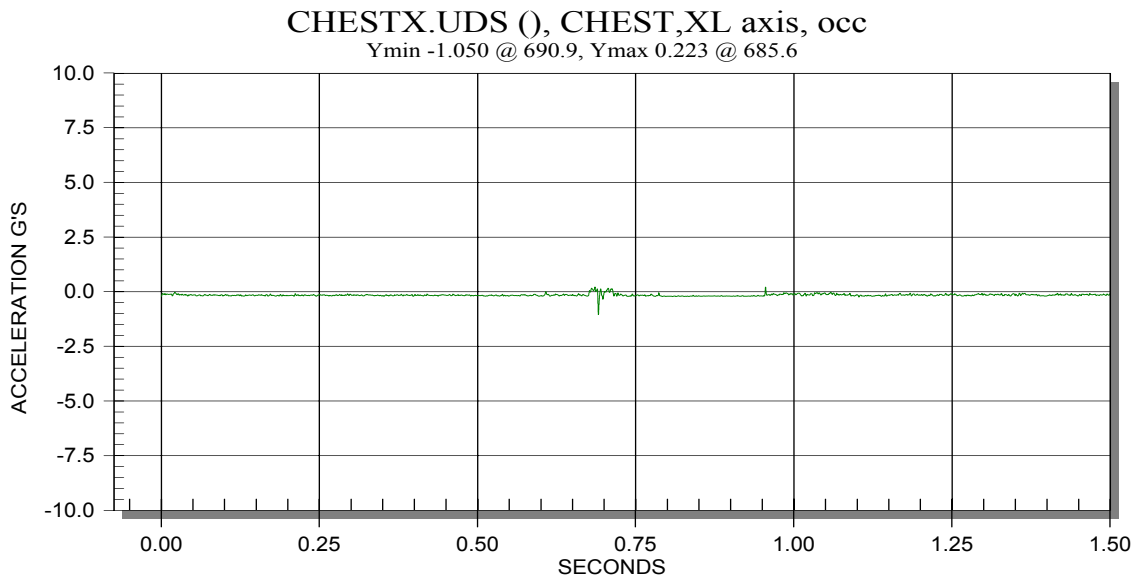


FIGURE C-15. CHEST X AXIS ACCELERATION (G's)—180-Hz FILTER

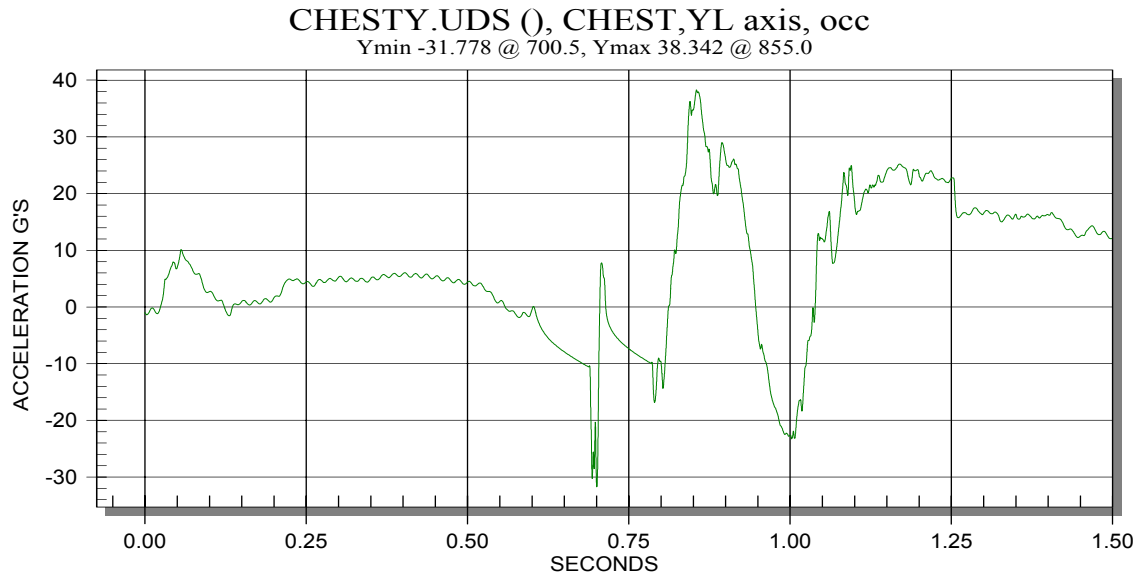


FIGURE C-16. CHEST Y AXIS ACCELERATION (G's)—180-Hz FILTER

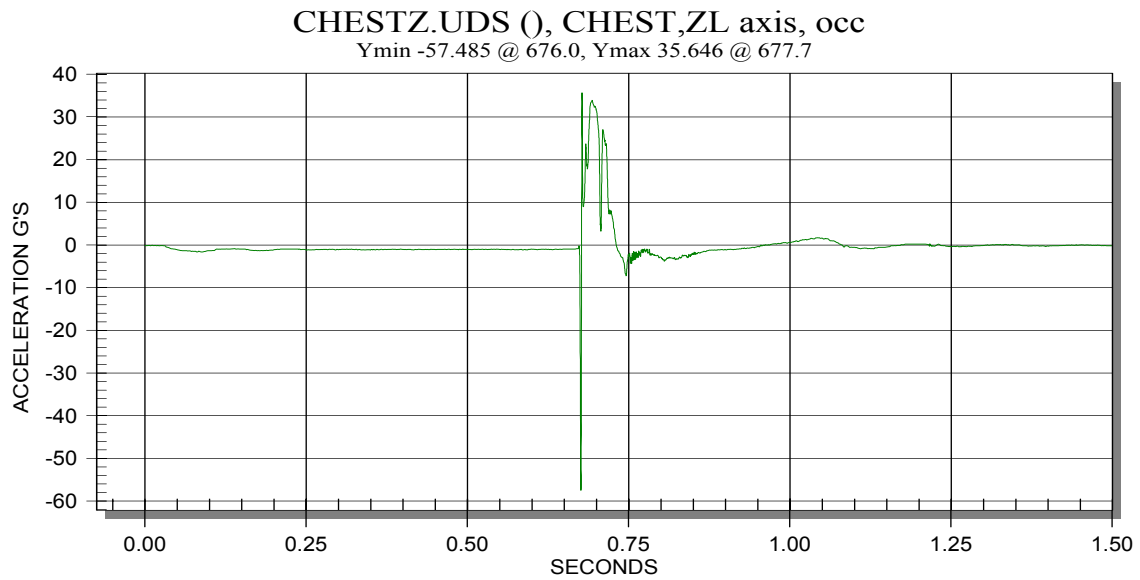


FIGURE C-17. CHEST Z AXIS ACCELERATION (G's)—180-Hz FILTER

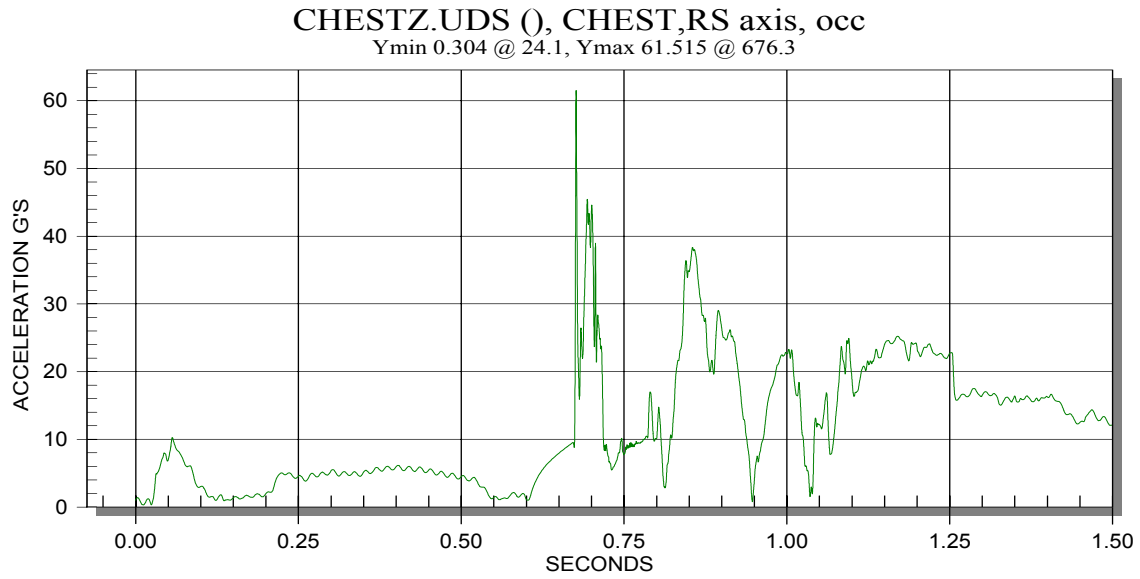


FIGURE C-18. CHEST RESULTANT ACCELERATION (G's)—180-Hz FILTER

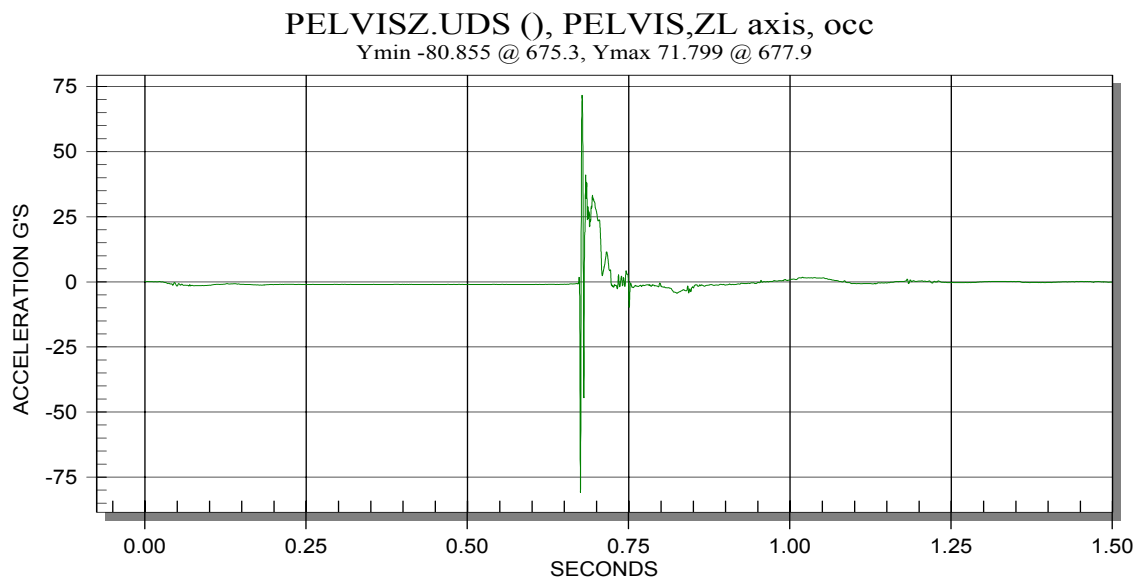


FIGURE C-19. PELVIS Z AXIS ACCELERATION (G's)—180-Hz FILTER

PLATFORMZ.UDS (), PELVIS,ZL axis, occ
Ymin -761.984 @ 669.6, Ymax 760.032 @ 669.9

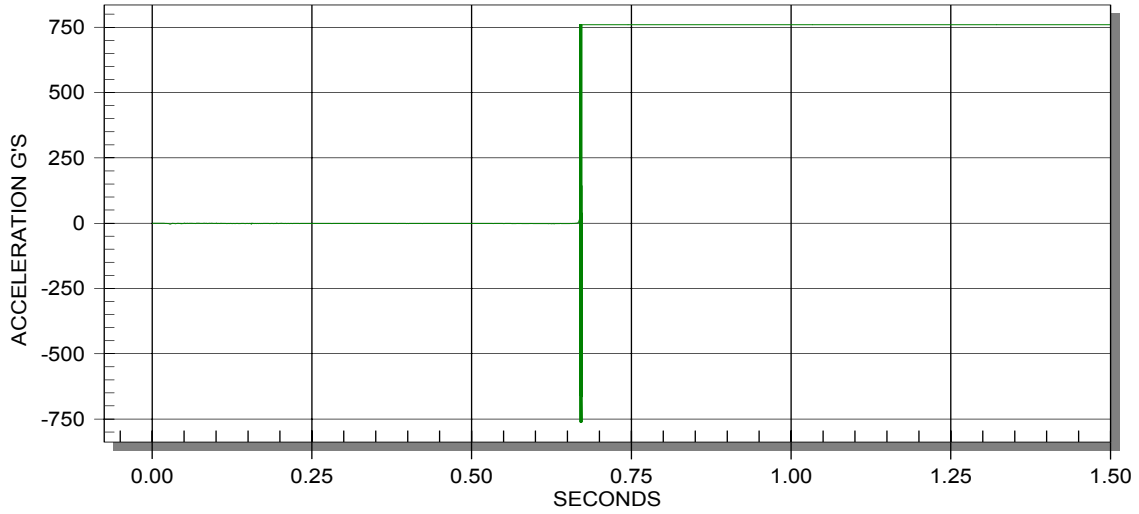


FIGURE C-20. PLATFORM Z AXIS ACCELERATION (G's)—CHANNEL FAILED

LUMBARFX.UDS (), SPINE,XL axis, occ
Ymin -13.737 @ 670.6, Ymax 3206.442 @ 670.0

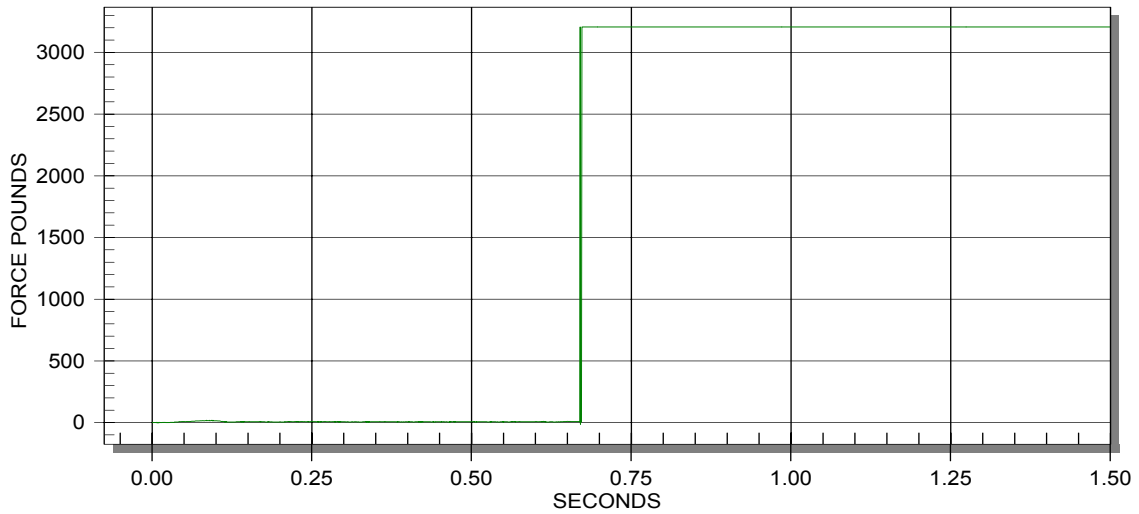


FIGURE C-21. LUMBAR LOAD CELL X AXIS FORCE (lb)—CHANNEL FAILED

LUMBARFY.UDS (), SPINE,YL axis, occ
Ymin -1.896 @ 8.3, Ymax 3209.746 @ 670.0

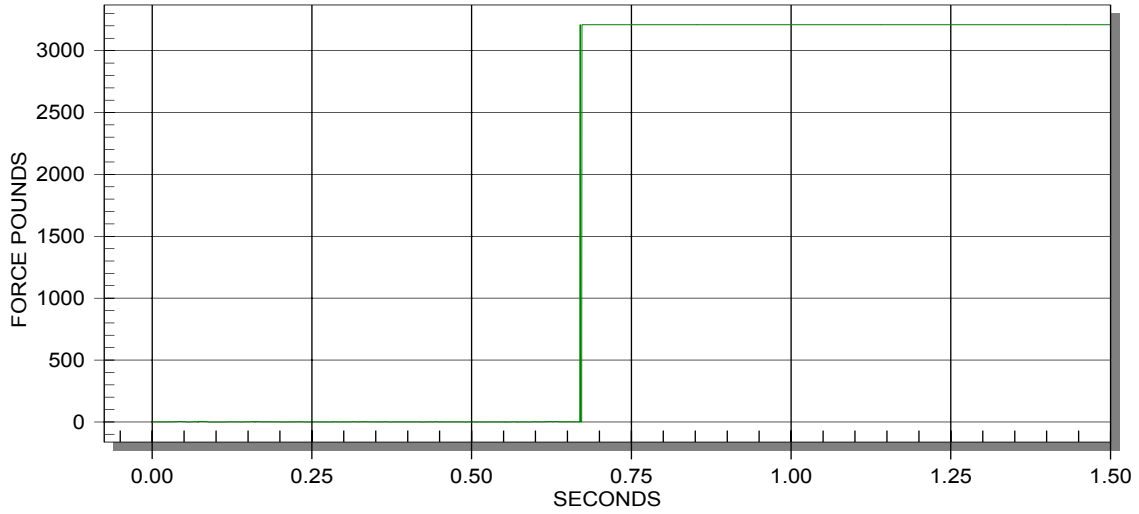


FIGURE C-22. LUMBAR LOAD CELL Y AXIS FORCE (lb)—CHANNEL FAILED

LUMBARFZ.UDS (), SPINE,ZL axis, occ
Ymin -16.749 @ 24.5, Ymax 5896.611 @ 672.8

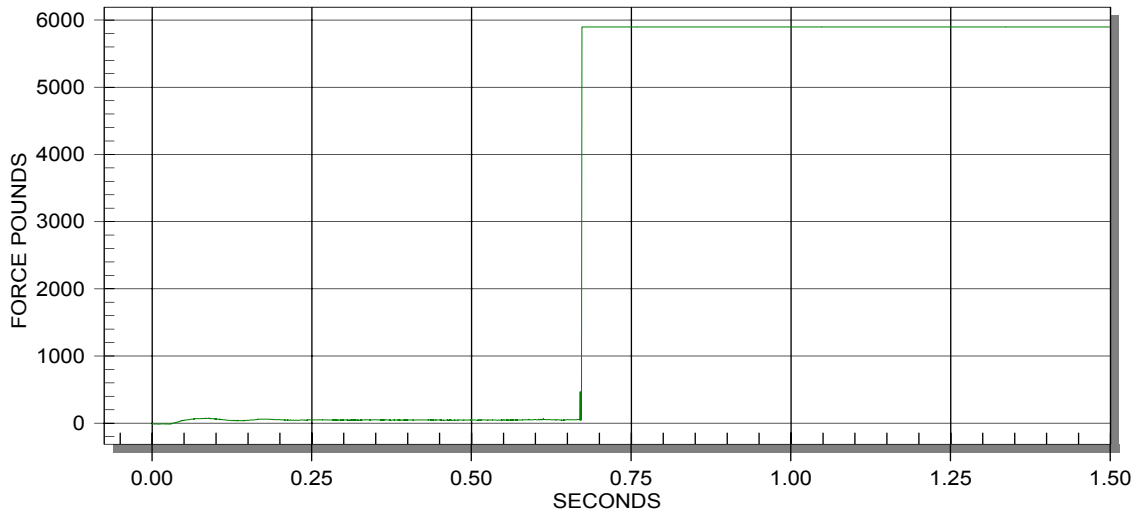


FIGURE C-23. LUMBAR LOAD CELL Z AXIS FORCE (lb)—CHANNEL FAILED

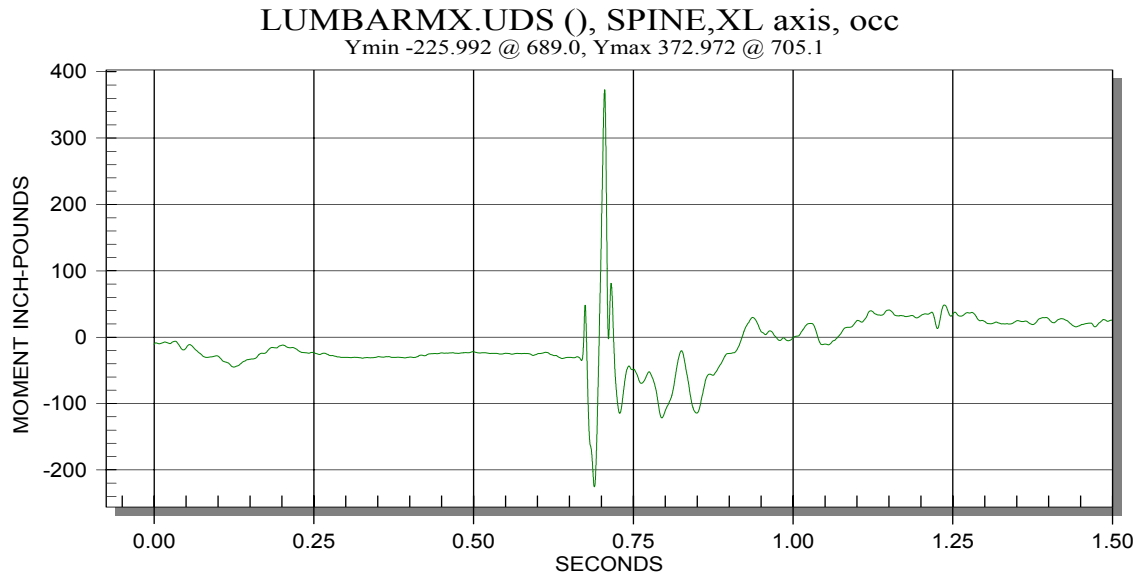


FIGURE C-24. LUMBAR LOAD CELL MOMENT X AXIS (lbs-in)—60-Hz FILTER

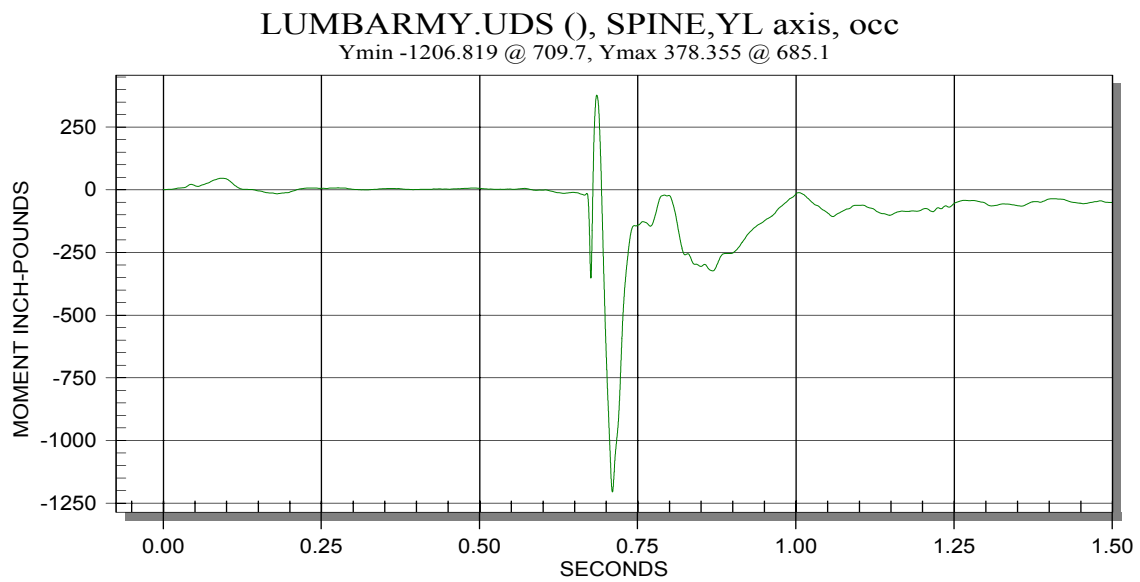


FIGURE C-25. LUMBAR LOAD CELL MOMENT Y AXIS (lbs-in)—60-Hz FILTER

LUMBARMZ.UDS (), SPINE,ZL axis, occ
Ymin -66.058 @ 1006.4, Ymax 62.864 @ 695.3

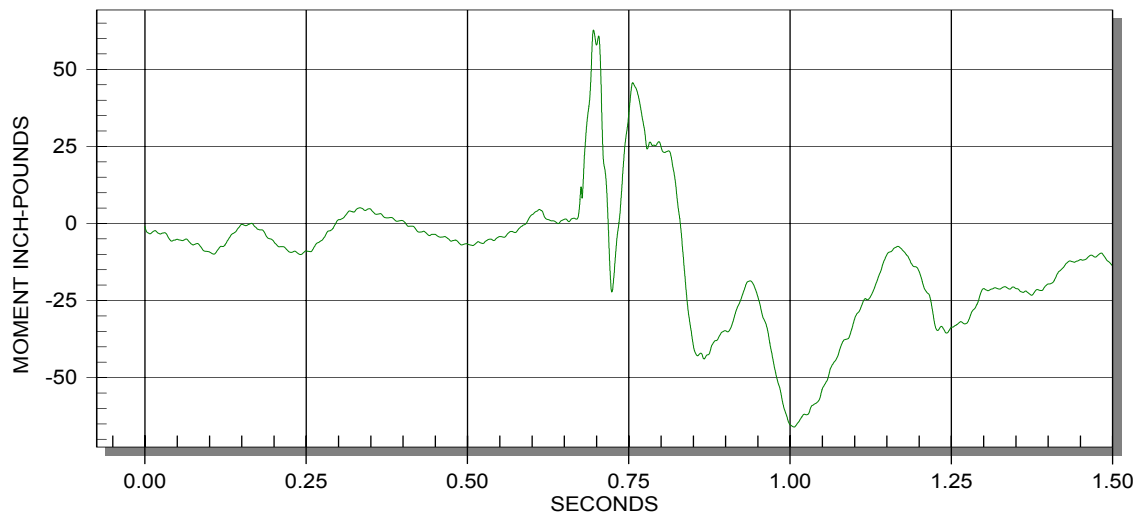


FIGURE C-26. LUMBAR LOAD CELL MOMENT Z AXIS (lbs-in)—60-Hz FILTER